FINAL REPORT

Novel Eulerian Two-phase Simulations for Burial Dynamics of Munitions Phase I

SERDP Project MR20-1478

SEPTEMBER 2020

Tian-Jian Hsu
Benjamin Tsai
Ali Salimi Tarazouj
University of Delaware

Julien Chauchat
Eduard Puig Montella
Cyrille Bonamy
LEGI, University of Grenoble – France

Distribution Statement A
This document has been cleared for public release

SERDP
DOD ▪ EPA ▪ DOE

This report was prepared under contract to the Department of Defense Strategic Environmental Research and Development Program (SERDP). The publication of this report does not indicate endorsement by the Department of Defense, nor should the contents be construed as reflecting the official policy or position of the Department of Defense. Reference herein to any specific commercial product, process, or service by trade name, trademark, manufacturer, or otherwise, does not necessarily constitute or imply its endorsement, recommendation, or favoring by the Department of Defense.

REPORT DOCUMENTATION PAGE

Form Approved
OMB No. 0704-0188

The public reporting burden for this collection of information is estimated to average 1 hour per response, including the time for reviewing instructions, searching existing data sources, gathering and maintaining the data needed, and completing and reviewing the collection of information. Send comments regarding this burden estimate or any other aspect of this collection of information, including suggestions for reducing the burden, to Department of Defense, Washington Headquarters Services, Directorate for Information Operations and Reports (0704-0188), 1215 Jefferson Davis Highway, Suite 1204, Arlington, VA 22202-4302. Respondents should be aware that notwithstanding any other provision of law, no person shall be subject to any penalty for failing to comply with a collection of information if it does not display a currently valid OMB control number.
PLEASE DO NOT RETURN YOUR FORM TO THE ABOVE ADDRESS.

1. REPORT DATE *(DD-MM-YYYY)*	**2. REPORT TYPE**	**3. DATES COVERED** *(From - To)*
10/09/2020	SERDP Final Report	9/18/2019 - 9/18/2021

4. TITLE AND SUBTITLE

Novel Eulerian Two-phase Simulations for Burial Dynamics of Munitions

5a. CONTRACT NUMBER
19-P-0114

5b. GRANT NUMBER

5c. PROGRAM ELEMENT NUMBER

6. AUTHOR(S)
Tian-Jian Hsu, Benjamin Tsai, Ali Salimi Tarazouj

University of Delaware

Julien Chauchat, Eduard Puig Montella, Cyrille Bonamy

LEGI, University of Grenoble – France

5d. PROJECT NUMBER
MR20-1478

5e. TASK NUMBER

5f. WORK UNIT NUMBER

7. PERFORMING ORGANIZATION NAME(S) AND ADDRESS(ES)
University of Delaware
259 Academy Street
Coastal Engineering Lab
Newark, DE 19716

8. PERFORMING ORGANIZATION REPORT NUMBER
MR20-1478

9. SPONSORING/MONITORING AGENCY NAME(S) AND ADDRESS(ES)
Strategic Environmental Research and Development Program (SERDP)
4800 Mark Center Drive, Suite 16F16
Alexandria, VA 22350-3605

10. SPONSOR/MONITOR'S ACRONYM(S)
SERDP

11. SPONSOR/MONITOR'S REPORT NUMBER(S)
MR20-1478

12. DISTRIBUTION/AVAILABILITY STATEMENT
DISTRIBUTION STATEMENT A. Approved for public release: distribution unlimited.

13. SUPPLEMENTARY NOTES

14. ABSTRACT
We present major results from a one-year SEED project to prepare a high fidelity two-phase numerical modeling framework SedFoam, for simulating scour burial in fluidization (sheet flow) condition, interaction with bedforms, and eventually investigating the effect of munition density. This proof-of-concept research effort is led by the objectives to (1) demonstrate that the Eulerian two-phase model SedFoam provides an effective modeling framework to directly resolve critical processes in scour burial, which cannot be easily achieved by conventional single-phase modeling approach, and (2) implement a few model enhancements for more physical-based closures in SedFoam to simulate processes that may lead to deep burial, namely, fluidization and bedforms.

15. SUBJECT TERMS
Sediment transport; Two-phase flow; Scour, Computational Fluid Dynamics, Unexploded Ordnance

16. SECURITY CLASSIFICATION OF:			**17. LIMITATION OF ABSTRACT**	**18. NUMBER OF PAGES**	**19a. NAME OF RESPONSIBLE PERSON**
a. REPORT	**b. ABSTRACT**	**c. THIS PAGE**			Tian-Jian Hsu
UNCLASS	UNCLASS	UNCLASS	UNCLASS	60	**19b. TELEPHONE NUMBER** *(Include area code)* 857-204-0336

Table of Contents

List of Figure

List of Acronyms

CFD	Computational Fluid Dynamics
KC number	Keulegan-Carpenter number
LEGI	Laboratoire des Écoulements Géophysiques et Industriels
OpenFOAM	Open Source Field Operation and Manipulation
SEED	SERDP Exploratory Development
UnMES	Underwater Munition Expert System
UXO	Unexploded Ordnance
VOF	Volume of Fluid

Keywords

Sediment transport; Two-phase flow; Scour, Computational Fluid Dynamics, Unexploded Ordnance

Abstract

We present major results from a one-year SEED project to prepare a high fidelity two-phase numerical modeling framework SedFoam, for simulating scour burial in fluidization (sheet flow) condition, interaction with bedforms, and eventually investigating the effect of munition density. This proof-of-concept research effort is led by the objectives to (1) demonstrate that the Eulerian two-phase model SedFoam provides an effective modeling framework to directly resolve critical processes in scour burial, which cannot be easily achieved by conventional single-phase modeling approach, and (2) implement a few model enhancements for more physical-based closures in SedFoam to simulate processes that may lead to deep burial, namely, fluidization and bedforms.

SedFoam is an open-source Eulerian two-phase model for sediment transport applications. By solving the mass and momentum equations for the water phase and fluid phase with closure on turbulence, particle stress and interphase momentum coupling, SedFoam resolves the full dynamics of sediment transport without the need to artificially separate transport into bedload and suspended load layers. Although SedFoam has been applied extensively to simulate current and wave driven sheet flow transport, plug flows, 3D scour around a cylindrical pile, these sediment transport problems are limited to the top 10 centimeters of the seabed and its application for deep burial processes, such as liquefaction, requires additional model enhancements. As a first step, we have made important progress to include dilatancy effects into SedFoam. Improved SedFoam can reproduce slow and rapid movement of an underwater avalanche due to negative and positive pore-pressure response caused by dilation and contraction of sediments resulting from different initial packing concentration observed in the laboratory experiment.

Major efforts are also devoted to proof-of-concept simulations. The two-phase model SedFoam is able to simulate piping as the onset of a 2D pipeline scour driven by waves similar to laboratory observation. Piping is a realistic scour onset process triggered by pore water flow passing underneath the structure because of the upstream-downstream pressure difference. This is an important demonstration of SedFoam's capability as typical single-phase CFD models for scour cannot allow the submerged object to be directly attached to or buried in the sand bed. Next, SedFoam is applied to simulate scour of a 3D horizontal short cylinder from low to high Keulegan-Carpenter (KC) number as a key step toward future simulation of UXO since horizontal short cylinder can be considered as the simplest UXO configuration having all the essential 3D characteristics. In the high KC number simulation similar to those cases observed in the field at Duck, NC (USA) when deep burial occurs, incoming boundary layer flow separation and horseshoe vortex are generated at the front of the cylinder. The vortices further extend to the two lateral faces of the cylinder as flow accelerates and leads to more significant erosion. Thirdly, we investigate SedFoam's capability to simulate migration and evolution of bedforms driven by waves. SedFoam is able to predict the evolution of ripple length and height subject to changing waves with good agreements with empirical ripple predictors. Moreover, the model is able to predict onshore ripple migration driven by onshore-velocity skewed waves similar to measure data.

In summary, we deliver a validated SedFoam model capable of accurately and efficiently simulating several key coupling mechanisms between hydrodynamics, sediment transport, underwater objects and seabed response. A more extensive research effort is needed to integrate these aforementioned key components consistently in the SedFoam modeling framework to create a new numerical modeling tool for scour burial of UXO. The new model can be used as a reliable analytical tool to study the mechanisms and thresholds for deep burial. Moreover, well-designed and extensive numerical simulations can be carried out to expand and to fill the data gaps of scour burial data in the Underwater Munition Expert System (UnMES).

Executive Summary

Introduction

Since the past decade, a great amount of research has been devoted to studying scour burial of munitions through laboratory experiment and field observations. Conventional knowledge of scour suggests that burial depth should not exceed about 1.2 UXO diameter and empirical formulae have been successfully developed and incorporated into Underwater Munition Expert System (UnMES). However, researchers have also noted that some observed burial depths, particularly in the field during energetic flow conditions, are significantly larger than 1.2 UXO diameter. Several mechanisms have been proposed to be responsible for deep burial, such as the occurrence of sheet flow, sheet flow accompanied by large horizontal pressure gradient due to passage of steep wave front (also called plug flow), residual and momentary liquefaction and migration of bedforms. A key scientific question is regarding the role of UXO density in the deep burial process, particularly when the aforementioned mechanisms mobilize, fluidize, or liquefy a thick layer of soil. While understanding these different mechanisms and obtaining data to predict the occurrence deep burial are currently relying on field and laboratory observations, it is highly desirable to create a high fidelity numerical model tool to predict scour burial of UXO, particularly under extreme condition or to fill the data gap in the wide parametric space.

Due to tightly coupled fluid-particle and inter-particle interactions covering the full range of particle concentration, developing a high fidelity model for scour burial processes is a very challenging subject. Conventional sediment transport models adopt a main assumption to separate the transport into the bedload and suspended load regions. The suspended load transport can now be highly resolved to investigate the interaction between turbulent eddies and suspended sediments. However, the bedload (or called near-bed load) transport is mainly parameterized by empirical formulas. A sediment transport model based on the two-phase flow formulation, on the other hand, is able to resolve the full transport processes and allows seamless integration of turbulence, particle-fluid, particle-particle interactions and seabed dynamics. Therefore, utilizing a two-phase model can avoid artificial separation of transport into near-bed load and suspended load layers. One of such two-phase models developed in the open-source OpenFOAM modeling framework is SedFoam.

In this study, SedFoam has been utilized and extended to carry out proof-of-concept simulations relevant to scour burial processes. As we will discuss in more details in the main report, our final goal is to develop a robust, computationally feasible, and high fidelity scour burial simulation tool based on two-phase modeling framework so that simulation results can be used to inform the Underwater Munition Expert System (UnMES) modeling framework for site management.

Objective

The *primary goal* of the proposed one-year SEED project is to prepare a novel two-phase numerical modeling framework, SedFoam, for simulating scour burial in fluidization condition (energetic sheet flow), interaction with bedforms, and eventually investigating the effect of munition density. We *hypothesize* that a next-generation numerical simulation tool that is able to address these outstanding issues in scour burial requires a Eulerian two-phase modeling framework. The *specific objectives* to prove the hypothesis are to (1) demonstrate that the Eulerian two-phase model SedFoam provides an effective modeling framework to directly resolve critical processes in scour, which cannot be easily achieved by conventional single-phase modeling

approach, and (2) with several model enhancements in SedFoam, it can be further extended to simulate aforementioned outstanding problems in scour burial of munitions. The following *technical objective* are executed in this SEED project:

1) Develop an effective sub-model in SedFoam for the effects of dilatancy/contraction on sediment transport.
2) Validate new enhancement with a series of benchmark cases relevant to the present scour burial problem.
3) Carry out proof-of-concept simulations relevant to laboratory and field conditions observed by SERDP-funded investigators.

Technical approach

SedFoam is an open-source Eulerian two-phase model for sediment transport applications. SedFoam framework has been shown in the past several years to be capable of simulating current and wave driven sheet flow transport, plug flows, 3D scour around a cylindrical pile and bedform migration/evolutions. SedFoam solves water phase and sediment phase by their own mass and momentum equations with interphase momentum coupling terms such as drag, pressure gradients and added mass. To model field-scale scour burial processes, Reynold-averaged (turbulence-averaged) methodology is primarily used and two turbulence closure options, k-ε model and k-ω model are available. The closure of particle phase stress is the most essential component in modeling near-bed sediment load. In SedFoam, different physics contributing turbulent suspension and particle stress are modeled according to sediment concentration. In lower concentration, short-lived particle collision and interaction between particles and turbulent eddies are the source of particle stress and it is modeled via turbulent viscosity via a two-equation closure and a kinetic component of particle stress as part of the kinetic theory of granular flow. Turbulence and particle stress in this lower sediment concentration range (volume concentration around 5~10%) plays an important role in suspending sediment and serves as a transition to dilute concentration (<5%) where suspension is fully taken over by vortices and turbulence. In moderate to high concentration (about 10% to 55%), particle stress is dictated by shear-induced intergranular interaction and it is modeled by the collisional component of kinetic theory or mu(I) rheology. Particle shear stress in this intermediate concentration range serves a vital role for the exchange of flow momentum between water phase and sediment. Meanwhile, the vertical gradient of particle pressure becomes the major suspension mechanism of sediment as turbulence is diminished close to the bed. Near-bed load transport occurring in this concentration range is key to scour, burial and ripple migration processes. In high concentration (>55%), sediment particles are nearly immobile and particle stresses serve a critical role to model the transition of fluid-like (plastic behavior) to solid-like (elastic) behavior and the overburden eventually is supported completely by the particle phase. The closure of particle stresses in this high concentration region of enduring contact is modeled empirically following the expected elastic behavior in the soil mechanics.

The existing particle stress closure in the high concentration region works reasonably well for most of the sediment transport applications investigated so far, which are mainly related to sediment transport near the top 10 cm of the sediment bed. To investigate deep burial problems which extend down to about 1 meter into the seabed, more comprehensive physics merging fluid mechanics with soil mechanics is necessary in order to model the transition from plastic (fluid-like) to elastic (solid) behavior of soil with large overburden. A major physics that is missing is shown to be the dilatancy effect. Dilatancy is the volume change in granular materials when subjected to shear

deformations. This volume change, dilation or compaction, is due to rearrangement of micro-structure and it leads to several important outcomes when modeling bulk granular/soil behavior. Firstly, it modifies the relationship between particle pressure (normal stress) and shear stress as particle concentration is below or above the critical state. This leads to a fluid-like or solid-like behavior even in dry granular materials. Secondly, for granular materials submerged in fluid, this volume change can greatly modify pore pressure and further stabilize or destabilize granular materials. In this proof-of-concept project, we develop a sub-model for dilatancy effects on sediment stress and excess pore pressure gradient.

The overall technical approach can be summarized into 4 tasks. Our Task 1 is mainly to set up generic and optimum model domains for simulating scour burial of 3D objects driven by waves (oscillatory flows) so that later we can more easily carry out proof-of-concept simulations. The efforts include three subtasks: a) we set up a model domain for simulating the scour of a vertical pile. In subtask b), we setup a model domain for simulating scour of a 3D short horizontal cylinder driven by oscillatory flow following the earlier laboratory experiments. This model setup is directly relevant to the proof-of-concept simulation in Task 4. In subtask c), we establish a simple model domain to test SedFoam's capability in simulating ripple evolution driven by waves as ripples/bedforms migration is considered to be another important factor causing burial. In Task 2, we carried out thorough literature reviews and the development of sub-models for dilatancy and pore-pressure feedback in SedFoam. The newly implemented sub-model is then tested with benchmark tests in Task 3, particularly for underwater avalanching in order to evaluate whether the sub-model is able to reproduce the expected dilatancy effects. Task 4 focuses on carrying out several proof-of-concept simulations relevant to scour burial processes and SERDP-supported observations. This task demonstrates evidence that SedFoam is capable of simulating essential processes relevant to scour burial and is ready for a full implementation toward a new research tool for scour burial of UXO.

Results and Discussion

Several key results resulting from this SEED project are briefly summarized here. In addition to SedFoam model enhancement for more complete physics for scour burial problems, we emphasize highlights from proof-of-concept simulations relevant to field and laboratory observed scour burial processes in order to illustrate future model development potential.

To ensure SedFoam is capable of simulating the mechanics associated with large erosion and deep burial processes, we have made important progress to include dilatancy effects into SedFoam as a first step. For wet soils, dilatancy and volume change can greatly modify pore pressure and further stabilize or destabilize the sediment. Improved SedFoam with dilatancy effect included can reproduce slow and rapid movement of underwater avalanche due to negative and positive pore-pressure response caused by dilation and contraction of sediments resulted from different initial packing concentration observed in the laboratory experiment. In addition to this fundamental improvement of SedFoam with more complete physics, the following achievements are related to proof-of-concept simulations.

In typical single-phase CFD models for scour, the submerged object/structure cannot be directly attached to or buried in the sand bed and a small gap has to be artificially introduced. Such limitation prevents the simulation of realistic scour onset triggered by pore water (seepage) flow passing underneath the structure caused by the upstream-downstream pressure difference, which is called piping in the literature. The two-phase model SedFoam is able to simulate piping as the

onset of a 2D pipeline scour driven by waves. At the early stage of the simulation with small waves, no scour is developed but the interaction between the incoming boundary layer flow (directed to the left) and the pipeline at this moment causes flow separation (Figure I(a)) at the left side of the pipeline. A weak excess pore pressure difference can be observed in the seabed which drives a small seepage flow toward the offshore direction. At a later stage when the waves become more intense (Figure I(b)), a strong flow separation at the offshore side of the pipeline causes much significant excess pore pressure difference and seepage flow in the seabed underneath the pipeline and we observe notable erosion and tunneling underneath the pipeline. The small gap allows high speed flow to pass through and lead to more significant erosion later. The capability of SedFoam to directly simulate the interaction between flow, sediment and object without artificial treatment is vital to the future model application to scour burial processes.

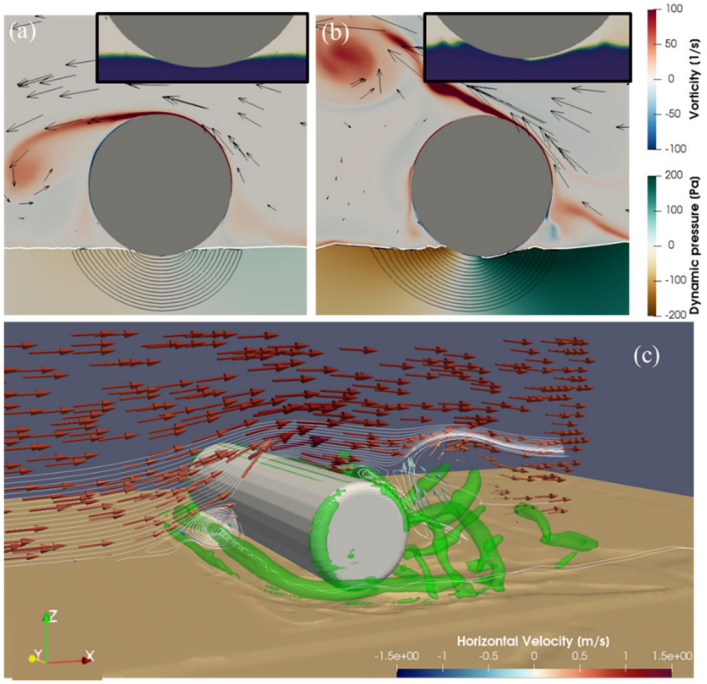

Figure I: Panel (a) and (b) are two snapshots of onset of scour via piping underneath a 2D pipeline (cylinder) driven by oscillatory flows. The flow field is signified by velocity vectors and vorticity. The color plot in the bed represents excess pore pressure and lines are streamlines of seepage flow. Two insets show enclosed view just below the pipe. Panel (c) shows a snapshot of flow field and scoured sediment bed around a 3D short cylinder driven by an oscillatory flow. The flow field is represented by the vectors and streamlines at the central plane and coherent vortices are visualized by iso-surface of the vortex vector |R|=25 (1/s).

SedFoam is created in the widely used OpenFOAM CFD framework and hence it is highly capable of simulating flow and vortices around a 3D object. Figure I(c) shows a simulation for scour around a 3D short cylinder (diameter 8 cm) driven by an oscillatory flow. It is evident that at this high Keulegan-Carpenter number (KC=55), similar to those cases observed in the field at Duck, NC (USA) when deep burial occurs, incoming boundary layer flow separation and horseshoe vortex are generated at the front of the cylinder. The vortices further extend to the two lateral faces of the

cylinder as flow accelerates and leads to more significant scour. Predicting this scour pattern is important as it later causes tiling of the cylinder as reported by laboratory experiments.

Bedforms are ubiquitous in coastal environments. The evolution and migration of bedforms can also cause burial and reemergence of UXOs. In this proof-of-concept study based on a two-phase modeling framework, we also investigate SedFoam's capability to simulate migration and evolution of bedforms driven by waves (oscillatory flows). SedFoam is capable of simulating ripple evolution due to changes in wave forcing. Figure II(a) shows SedFoam simulation of reduction of ripple size due to reducing wave period via splitting. The ripple profile was initialized (t=0 sec) with the profile from a previous simulation with orbital velocity amplitude U_m=0.48 m/s and T=5 sec (orbital length d_0=0.76 m) with ripple length l_0=0.46 m and ripple height h_0=0.0782 m (h_0/l_0=0.17). Due to reduction of wave period to T=3 sec (d_0=0.46 m), ripple length was reduced by splitting. The final ripple length and height at t=250 sec are of l_f=0.23 m and h_f=0.0391 m. Figure II(b) shows the formation of ripples from a nearly flat bed. The ripple profile was initialized with a bed profile from a previous sheet flow simulation with U_m=1.5 m/s and T=5 sec (Shields parameter about 1.5). The simulation is then carried out with U_m=0.48 m/s and T=5 sec. At t=300 sec, the flat bed evolves into three ripples in the domain with ripple length l_0=0.46 m and ripple height h_0=0.0782 m, nearly identical to that at t=0 in Figure II(a). Overall, the simulated final ripple lengths and heights in these two cases are in good agreement with empirical formulas.

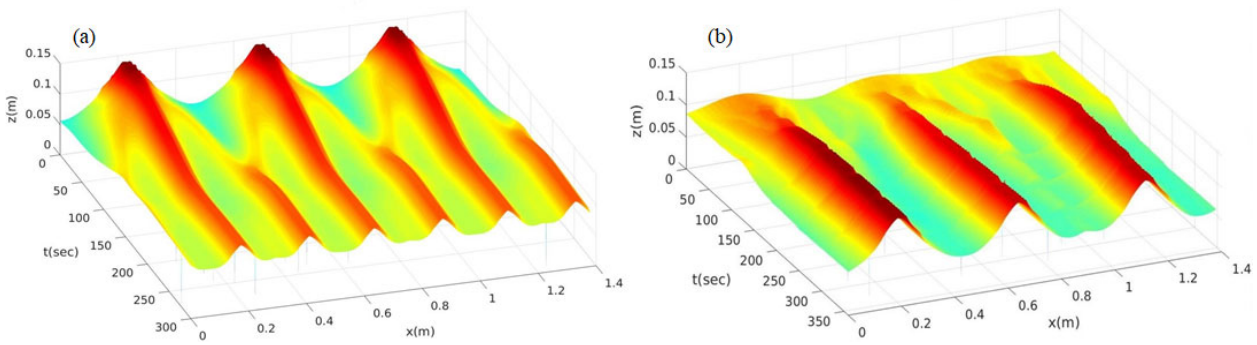

Figure II: (a) Ripple evolution due to reduction of wave period. (b) Ripple formation from a nearly flat bed.

Implications for Future Research Benefits

Through the support of the 1-year SEED project, we deliver a validated SedFoam model capable of accurately and efficiently simulating several key coupling mechanisms between hydrodynamics, sediment transport, underwater objects and seabed response. The model is successfully extended to capture dilatancy effects on sediment transport. The new sub-model has been validated with several benchmark cases. Several proof-of-concept simulations show that SedFoam is capable of simulating scour driven by waves with realistic onset through piping and backfilling, scour of a 3D short cylinder at KC number similar to the field observation reported at Duck, NC. The model is also capable of simulating migration and evolution of bedforms.

We have fulfilled the project objectives to demonstrate that the Eulerian two-phase model SedFoam provides an effective modeling framework to directly resolve critical processes in scour, which cannot be achieved by conventional single-phase modeling approach. Moreover, several model enhancements and proof-of-concept simulations provided promising advancement for SedFoam and the model is now ready for a full implementation toward a new research tool for scour burial of UXO.

The full implementation in SedFoam to solve deep burial problems allow the investigation of two critical physical mechanisms responsible for scour burial: 1) Mechanisms triggering deep scour burial (~1 meter), and 2) Effect of UXO density. We hypothesize that deeper burial is related to UXO density, however, a mechanism (or mechanisms) must first exist to fluidize or liquefy the sediment bed. We plan to use a fully equipped SedFoam numerical modeling framework to investigate this important and challenging problem. Essentially, we propose to use SedFoam as a simulation tool to create parameterizations for liquefaction potential, burial depth as a function of UXO density, and other nondimensional flow parameters. A full understanding of deep burial certainly requires extensive field observations and available measured data will be used to validate our numerical model. Well-designed numerical experiments can be then carried out to fill the parameter space, either for higher quality interpolation within the range of the field observation, or for extrapolation to extreme events that are outside the range of field observation. Simulation data will be made available to train the existing expert system UnMES for scour burial prediction.

1. Objective

The *primary goal* of the proposed one-year SEED project is to prepare a novel two-phase numerical modeling framework, SedFoam, for simulating scour burial in energetic sheet flows (fluidization of seabed surface), interaction with bedforms, and eventually investigating the effect of munition density. As summarized in Rennie (2017), these are outstanding processes critical to scour burial prediction while existing computer simulation models' capability toward these critical processes are lacking. We *hypothesize* that the next-generation numerical simulation tool that is able to address these outstanding scour burial issues require a Eulerian two-phase modeling framework. For this one-year proof-of-concept project, the *specific objectives* to prove the hypothesis are to (1) demonstrate that the Eulerian two-phase model SedFoam provides an effective modeling framework to directly resolve critical processes in scour, which cannot be achieved by conventional single-phase modeling approach, and (2) with several model enhancements in SedFoam, it can be further extended to simulate aforementioned outstanding problems in scour burial of munitions. By achieving these two objectives in the SEED project, we can ensure that SedFoam modeling framework is sufficiently robust to include more complex sub-models for sediment stress and pore-pressure response in order to deal with the sophisticated dynamics during the transition between fluid-solid behavior in sediment bed. Moreover, several successful proof-of-concept simulations allow us to evaluate and ensure that it is computationally feasible to simulate field-scale relevant problems similar to those observed by other SERDP-supported studies. In summary, this report will document our effort in achieving these two objectives and leading to a significant risk reduction for SERDP to further invest more resources for the future development of this new modeling tool.

To achieve the project goal and objectives, the following *technical objective* are executed in this SEED project:

1) Develop an effective sub-model in SedFoam for the effects of dilatancy/contraction on sediment transport.
2) Validate new enhancements with a series of benchmark cases relevant to the present scour burial problem.
3) Carry out proof-of-concept simulations relevant to laboratory and field conditions observed by SERDP-funded investigators.

2. Background

In the past decade, there have been many important observations reported by investigators supported by SERDP and the Mine Burial Program (Wilkens and Richardson 2007) on the burial depth of munitions (e.g., Cataño-Lopera and Garcia 2006; Cataño-Lopera et al. 2007; Demir and Garcia 2007; Friedrich et al. 2016; Calantoni 2016; Traykovski and Austin 2017). A complete summary has been provided in a recent report for the development of Underwater Munition Expert System (UnMES) by Rennie (2017). According to conventional knowledge of scour, burial depth should not exceed about 1.2 UXO diameter and empirical formulae have been successfully developed (Friedrichs et al. 2016) and incorporated into UnMES. However, it was noted in Rennie (2017) that some observed burial depths, particularly in the field during energetic flow conditions, are significantly larger than 1.2 UXO diameter. For instance, Traykovski and Austin (2017) observed burial depth up to 4 UXO diameters near Martha's Vineyard Coastal Observatory. Calantoni (2016) measured burial depth up to about 7.5 UXO diameters during a storm event at Duck, NC.

Researchers have suggested several mechanisms that may be responsible for deep burial. The first mechanism is due to the occurrence of sheet flow, or called "fluidization" (Rennie et al. 2017). Sheet flow occurs when the nondimensional bottom shear stress (Shields parameter) is larger than about 0.5. High bottom shear stress fluidized a mobile sediment layer on the order of 10 to 50 grain diameters, which is typically no more than a few centimeters. Hence, it is likely that sheet flow alone may not explain the deep burial, which can be up to several tens of centimeters to a meter. Foster et al. (2006) demonstrated that in sheet flow conditions under the passage of steep breaking wave front, it was accompanied by large horizontal pressure gradient. This intense sediment transport process is called plug flow and the resulting erosion depth can be several times larger than that in pure sheet flow condition (Cheng et al. 2017). Recently, Klammler et al. (2019) further showed that deep burial can be caused by residual and momentary liquefaction, which is widely recognized in marine soil mechanics. More importantly, they also demonstrated the possibility that during scour burial in the ocean, all of the above mechanisms can co-exist and interact nonlinearly with munition density. Essentially, when a sufficiently thick layer of sediment is fluidized or mobilized, sediment (granular) bed behaves like a dense fluid and the relative densities between the munition and sediment particle may play a significant role in the resulting burial depth (Calantoni 2016). Finally, deep burial can also be caused by migrating bedforms (Traykovski and Austin 2017) in regions where bedform evolution and migration are known to be active. Bedforms in wave-dominant environments can reach a length up to about 1.5~2.5 m and a height up to about 30~50 cm (Traykovski et al. 1999) and hence they have the potential to completely bury UXO. Bedforms in current-dominant condition can be even larger. Although there are many empirical bedforms geometry predictors, most of them are limited to equilibrium condition. Bedforms can migrate toward the direction of wave velocity skewness and asymmetry (Traykovski 2007) and typical migration speed can be up to about several tens of centimeters per hour. Therefore, bedforms are highly dynamic seafloor features that can bury UXO for a period of time. In the field condition, observed deep burial may be associated with bedform migration and this mechanism is completely different from the scour burial processes discussed earlier.

Due to tightly coupled fluid-particle and inter-particle interactions covering the full range of particle concentration, developing a high fidelity model for scour burial processes is a challenging subject. In moderate to high concentration, transport is dominated by various types of intergranular

interactions from intermittent collisions to enduring contacts. Through contributions from both particle inertia and interstitial fluid viscosity, various rheological closures are required (e.g., Lun et al. 1984; Boyer et al. 2011). When sediment concentration becomes lower, transport often becomes increasingly dominated by turbulence, while the turbulent eddies are also affected by the particles. Due to these highly complex processes, conventional sediment transport models split the transport into the bedload and suspended load regions. The suspended load transport can now be highly resolved to investigate the interaction between turbulent eddies and suspended sediments. However, the bedload (or called near-bed load) transport is often parameterized with empirical power law formula. While these conventional models had made progress in predicting sediment transport, including scour processes (e.g., Baykal et al., 2015), it is difficult to apply them for munition burial problems because of the inherited assumption to treat transport layers of different concentrations in an artificial manner. An accurate numerical model that is able to resolve bedform evolution and migration is also scarce (Marieu et al. 2008; Chou and Fringer 2010).

A sediment transport model based on the two-phase flow formulation, on the other hand, is able to resolve the full transport processes and allows seamless integration of turbulence, particle-fluid, particle-particle interactions and seabed dynamics. Therefore, utilizing a two-phase model can avoid artificial separation of transport into near-bed load and suspended load layers. One of such two-phase models is SedFoam (Cheng et al. 2017; Chauchat et al. 2017). SedFoam is a Eulerian two-phase model for sediment transport applications developed in the open-source OpenFOAM modeling framework. SedFoam has been shown in the past several years to be capable of simulating current and wave driven sheet flow transport (Cheng et al. 2017; Kim et al. 2018, 2019; Cheng et al. 2018). In the study of Cheng et al. (2017), SedFoam is applied to study the mechanism driving large erosion depth in sheet flow due to large horizontal pressure gradient. Model results suggested that large horizontal gradient drives plug flow and leading to a type of shear instabilities of the concentrated transport layer that further enhances transport layer thickness and transport rate. Sedfoam is built in the Openfoam framework and hence it is relatively easy to add other capabilities in the two-phase solver. For instance, we expanded SedFoam for 3D large-eddy simulation capability to better resolve flow instabilities during flow reversal under waves in sheet flows (Cheng et al. 2018). SedFoam is also extended to resolve air-water interfaces using VOF type methods in order to directly include surface wave processes in modeling sediment transport (Kim et al. 2018, 2019). Recently, SedFoam has been extended to simulate 3D scour around a cylindrical pile (Nagel et al. 2020) and wave-driven bedform evolutions (Salimi-Tarazouj et al. 2020a,b).

In this study, SedFoam has been utilized and extended to carry out proof-of-concept simulations relevant to scour burial processes. As we will discuss in more details in the Conclusion and Implication for Future Research section, our final goal is to develop a robust, computationally feasible, and high fidelity scour burial simulation tool based on two-phase modeling framework so that simulation results can be used to inform the Underwater Munition Expert System (UnMES) modeling framework (Rennie 2017) for site management.

3. Materials and Method

3.1 SedFoam Model

The Eulerian two-phase model, SedFoam, solves water phase and sediment phase by their own mass and momentum equations with coupling terms such as drag, pressure gradients and added mass. In this study, Reynold-averaged (turbulence-averaged) methodology is used and hence for the closure of fluid Reynolds stress, eddy (turbulent) viscosity assumption is adopted and two turbulence closure options, k-ε model and k-ω model can be used. The closure of particle phase stress is the most essential component in modeling near-bed load and seabed stability. In SedFoam, different physics contributing particle stress are modeled according to sediment concentration. In lower concentration, short-lived particle collision and interaction between particles and turbulent eddies are the source of particle stress and it is modeled via a kinetic component as part of the kinetic theory of granular flow (Ding & Gidaspow 1990; Hsu et al. 2004). Particle stress in this lower sediment concentration range (around 5~10% in volumetric concentration) plays an important role in suspending sediment and serves as a transition to dilute concentration (<5%) where suspension is fully taken over by turbulence. In moderate to high concentration (about 10% to 55%), particle stress is dictated by shear-driven intergranular interaction and it is modeled by the collisional component of kinetic theory (Jenkins and Hanes 1998) or μ(I) rheology (Boyer et al. 2011). Particle shear stress in this intermediate concentration range serves a vital role for the exchange of flow momentum between water phase and sediment phase and the water phase velocity experiences significant "friction" due to the presence of sediment phase (often phrased as "roughness"; Cheng et al. 2018). From the soil mechanics perspective, this region is where particle stress shows a "plastic" behavior. Meanwhile, the vertical gradient of particle pressure generated by horizontal shear becomes the major suspension mechanism of sediment as turbulence is diminishing close to the bed. In high concentration (>55%), sediment particles are nearly immobile (creeping motion) and particle stresses serve a critical role to model the transition of fluid-like to solid-like behavior and the overburden eventually is supported completely by the particle phase. The closure of particle stresses in this high concentration region of enduring contact is modeled empirically following the elastic behavior expected in the soil mechanics.

The existing particle stress closure in the high concentration region works reasonably well for most of the sediment transport applications investigated so far, which are mainly related to sediment transport near the top 10 cm of the sediment bed. To investigate deep burial problems which extend down to about 1 meter into the seabed, more comprehensive physics merging fluid mechanics with soil mechanics is necessary in order to model the transition from plastic (fluid-like) to elastic (solid) behavior of soil with large overburden. A major physics that is missing is the dilatancy effect. Dilatancy is the volume change in granular materials when subjected to shear deformations. This volume change, dilation or compaction, is due to rearrangement of micro-structure and it leads to several important outcomes when modeling bulk granular/soil behavior. Firstly, it modifies the relationship between particle pressure (normal stress) and shear stress as particle concentration is below or above the critical state. This leads to a fluid-like or solid-like behavior even in dry granular materials. Secondly, for granular materials submerged in fluid, this volume change can greatly modify excess pore pressure and further stabilize or destabilize granular materials. We like to point out that the physics of dilatancy and the pore-pressure response occur in the micro-structure of soil skeleton, which is theoretically within the Eulerian averaging scale. Therefore, they cannot be directly resolved by the present modeling approach and sub-grid closure models are needed.

In this proof-of-concept project, we develop a relatively simple sub-model for dilatancy effects on sediment stress and excess pore pressure gradient. The model captures the known effect of dilatancy from laboratory observations, namely, dilation of initially densely packed sediments experiences enhanced apparent friction due to microstructure rearrangement and suction of pore water and on the other hand, contraction of initially loosely packed sediments experiences reduced apparent friction due to microstructure rearrangement and expulsion of pore water. The new model is benchmarked with laboratory experiment on underwater avalanching with good agreement (see Results and Discussion section). In the Conclusion and Implication for Future Research section, we will propose a more complete sub-models for dilatancy and pore-pressure feedback for soil in the field condition (soil with a small amount of air) so that future SedFoam can fully simulate partially-drained condition, and also allow modeling toward unsaturated soil.

3.2 Approach and Tasks

In this project, the methodology that we adopted to fulfill the specific objectives can be summarized into 4 main tasks and a flow chart is provided in Figure 1. Task 1 is mainly to set up generic and optimum model domains for simulating scour burial of 3D objects driven by waves (oscillatory flows) so that later we can extend the set up for proof-of-concept simulations more easily. The efforts include three subtasks: a) we setup a model domain for simulating the scour of a vertical pile driven by oscillatory flow by directly modifying our recently published work for steady flow (Nagel et al. 2020). Although this model set up is not directly related to munition, the domain arrangement and boundary conditions are still the basic requirement for future extension and it is an important exercise for the graduate students' modeling experience using complex mesh. In subtask b), we set up a model domain for simulating the scour of a 3D horizontal short cylinder driven by oscillatory flow at low Keulegan-Carpenter number (KC=4.8) following the earlier laboratory experiments reported by Demir and Garcia (2007). This model setup is directly relevant to the proof-of-concept simulation in Task 4. Major highlights of the model simulation will be presented in Section 4. In subtask c), we set up a simple model domain to test SedFoam's capability in simulating ripple evolution driven by waves as ripples/bedforms migration is considered to be another important factor causing burial.

Meanwhile, we also carried out a thorough literature review and the development of sub-models for dilatancy and pore-pressure feedback in SedFoam (Task 2). This task is led by co-PI Chauchat and his postdoc in LEGI, University of Grenoble – Alpes benefiting from their extensive experience in granular rheology. The newly implemented sub-model is immediately validated with benchmark tests proposed in Task 3. In section 4, we focus on reporting results for underwater avalanches in order to evaluate whether the sub-model is able to reproduce the expected dilatancy effects. As shown in the flow chart (Figure 1) Task 2 and Task 3 constitute an iterative procedure in order to develop the most effective sub-model. Another major results achieved Task 2 and 3 relevant to scour burial processes is onset of scour via piping, which will be discussed in Section 4. Task 4 focuses on carrying out several proof-of-concept simulations relevant to scour burial processes and SERDP-supported observations. This task shall demonstrate evidence that SedFoam is capable of simulating essential processes relevant to scour burial and it is ready for a full implementation toward a new research tool for scour burial of UXO. Major highlights from this task will also be presented in Section 4.

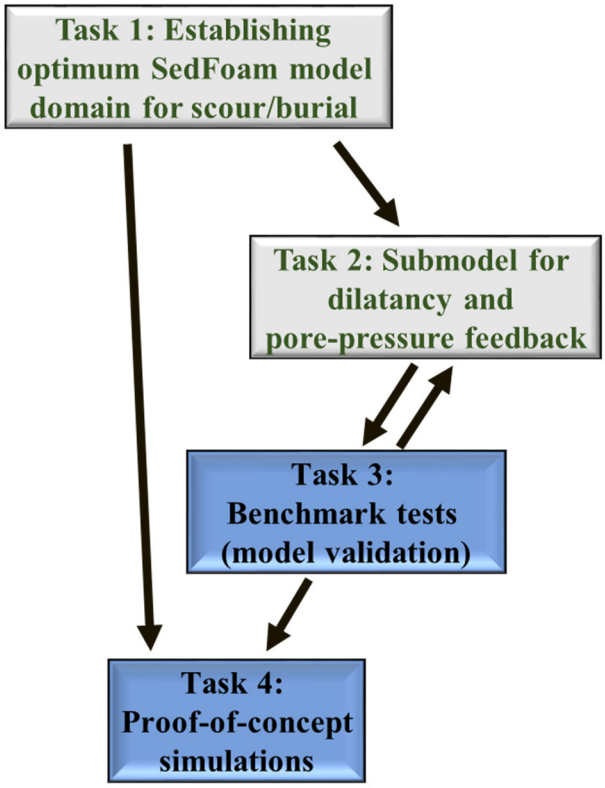

Figure 1: Flow chart for the four major Tasks proposed in this project.

4. Results and Discussion

4.1 Scour of a 3D short cylinder in low KC number – generic domain setup (Task 1)

Establishing SedFoam's capability to simulate the scour of a 3D short horizontal cylinder is a key step toward future simulation of UXO since a horizontal short cylinder can be considered as the most generic UXO configuration having all the essential 3D characteristics. From the technical perspective, this model configuration also allows us to iterate on the most numerically accurate and stable unstructured mesh setup. We specify the cylinder size and flow condition identical to a case of KC=4.8 and Shields parameter of 0.057 reported in the laboratory experiment by Demir and Garcia (2007). The wave motion is of velocity amplitude 0.2 m/s and wave period 3 sec. The short cylinder is of length 0.25 m and diameter 0.125 m in a rectangular prism model domain of 1.25 m in length, 0.8 m in width and 0.625 m in height. The short cylinder sits over a sand bed with a thickness of 0.125 m. In the entire 3D rectangular domain, high numerical resolution near the water-sediment interface is implemented (see Figure 2(a)). Near the cylinder, the mesh size is reduced to 2.5 mm in two horizontal directions and 0.83 mm in vertical direction (Figure 2(b)).

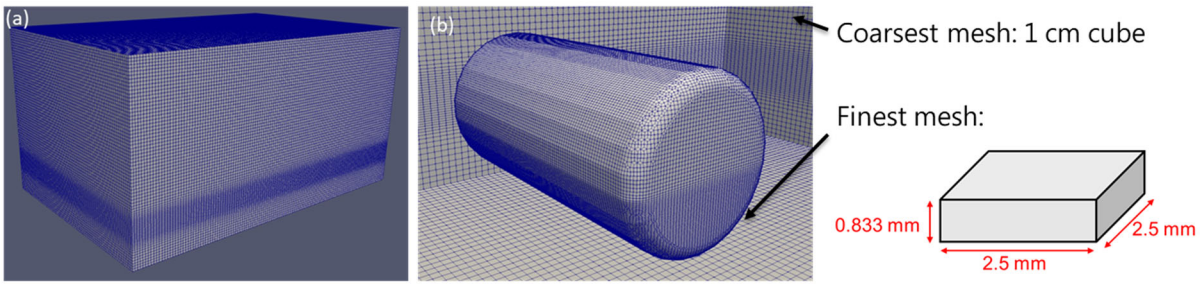

Figure 2: 3D model domain for scour of a short cylinder in oscillatory flow. The 3D unstructured mesh is generated using open-source cfMesh in the OpenFOAM framework. Panel (a) shows the entire 3D rectangular domain with high resolution near the water-sediment interface. Panel (b) shows a zoom-in view of the mesh near the short cylinder and smallest rectangular mesh used in this simulation.

Figure 3 shows a snapshot of flow field (see streamlines and velocity vectors) at the wave crest of the 3rd wave in the simulation. The most intriguing feature is the strong flow acceleration as flow approaches the two lateral faces of the cylinder, which triggers intense 3D vortices near the corner close to the sediment bed. These corner vortices are clearly responsible for the small depressions form below the cylinder. According to Demir and Garcia (2007), capturing this feature is important as the small corner scour holes can be further enlarged as the scour continues to move to the center and eventually causes tilting, sinking and burial of the object. Figure 4 shows a snapshot at the wave trough of the 3rd wave. We observe similar vortex patterns at the cylinder corner and here we further visualize the vortices using iso-surface of vorticity in the x and y directions. These vortices are associated with sharp pressure gradients at the end of the short cylinder (e.g., flow separation) but are further fueled with vorticity in the boundary layer from the cylinder surface. In Figure 5, we can see that the scour holes become deeper in the 4th wave. Simulations presented here are promising and further extensions for higher KC number and Shields parameter similar to field observations will be presented Section 4.5.

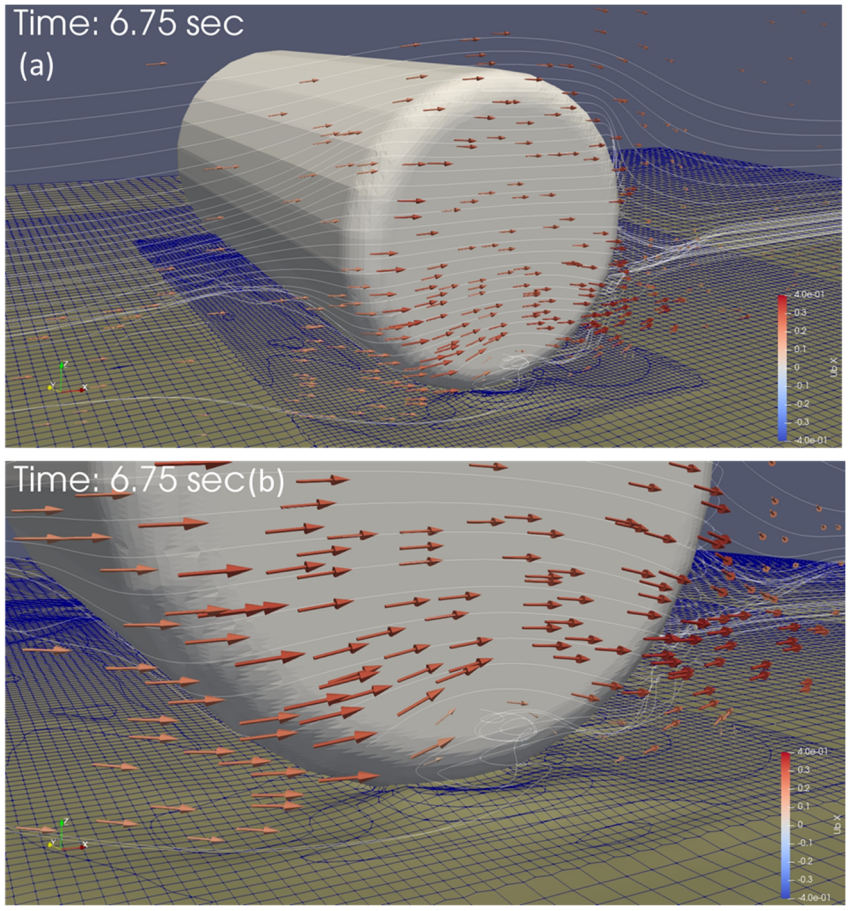

Figure 3: (a) A snapshot of velocity field, streamline and bathymetry viewing the right corner of the short cylinder at wave crest of the third period. Panel (b) shows a zoom-in view close to the sediment bed.

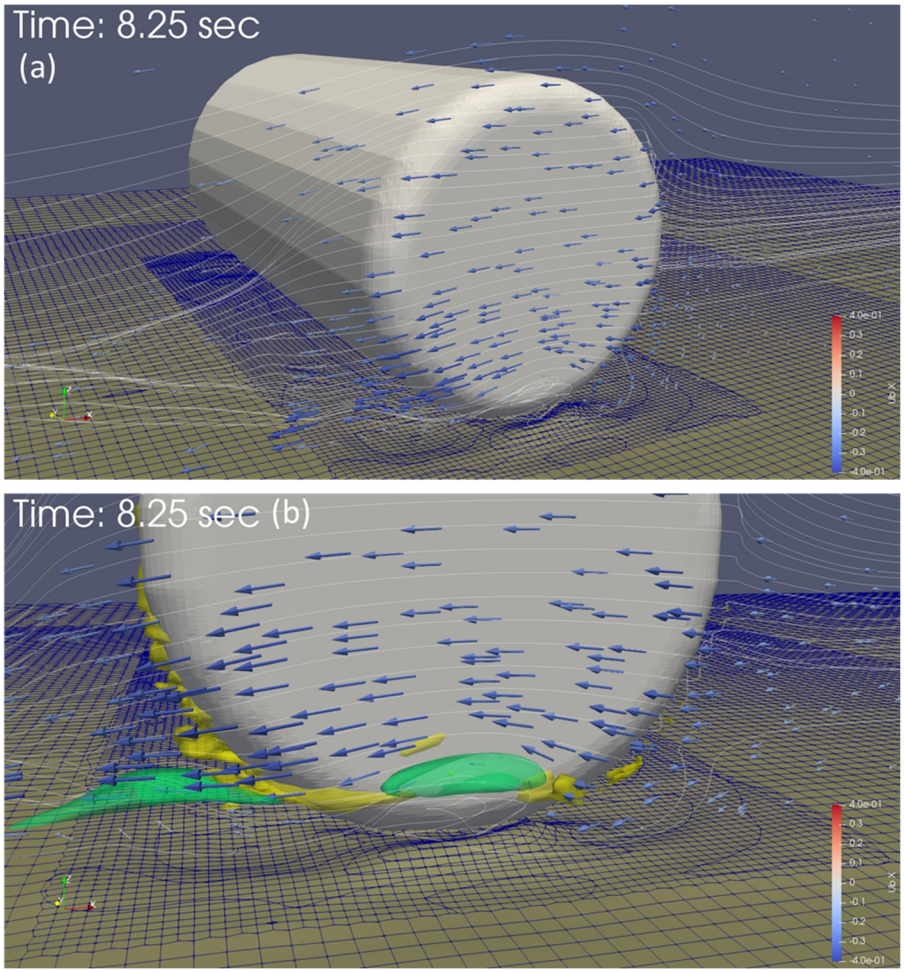

Figure 4: (a) A snapshot of velocity field, streamline, and bathymetry viewing the right corner of the short cylinder at wave trough of the 3rd period. Panel (b) shows a zoom-in view close to the sediment bed. Vortices structure is visualized by streamwise vorticity (ω_x, green) and spanwise vorticity (ω_y, yellow).

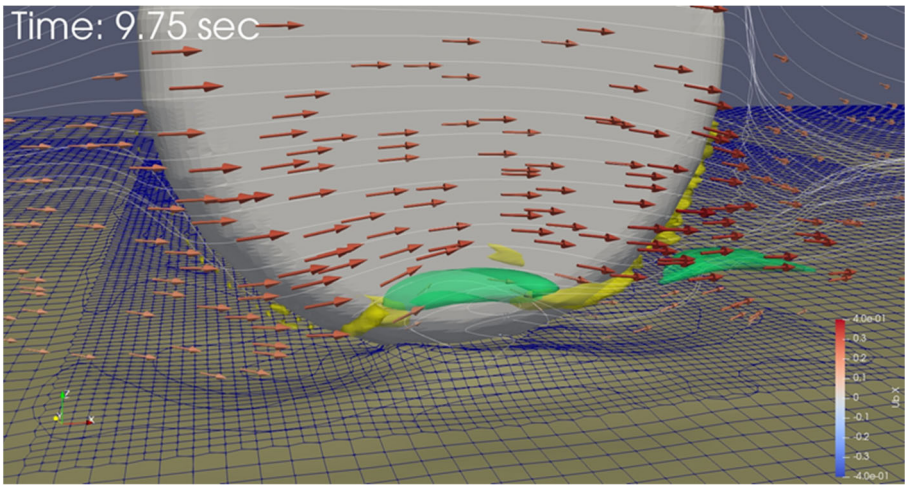

Figure 5: Zoom-in view close to the sand bed during the wave crest of 4th period. Comparing the bathymetry with Figure 3(b), the scour hole becomes deeper. Vortices structure is visualized by streamwise vorticity (ω_x, green) and spanwise vorticity (ω_y, yellow).

4.2 Ripple evolution (Task 1)

SedFoam's capability to simulate ripple migration driven by a velocity-skewed wave has been validated with detailed laboratory experiments reported by van der Werf et al. (2007) with very good agreement. More insight into onshore ripple migration and model validation will be presented along with other wave conditions in Section 4.7. As generic model domain setup in this section, we will focus on presenting two cases for predicting ripple evolution due to changing wave condition. The final ripple geometry in each run is compared with widely used ripple predictors.

SedFoam is able to simulate the formation of wave orbital ripples from a predominant flat-bed sheet flow condition as wave energy reduces. As shown in Figure 6, the simulation is initialized with a predominant flat-bed obtained previously from a sheet flow simulation with sand grain size d=0.44 mm subject to a simple harmonic wave motion of a large velocity amplitude U_0=1.5 m/s and wave period T=5 sec (mobility number ψ=316). At t>0, the wave velocity amplitude is reduced to U_0=0.48 m/s while maintaining the same wave period. The resulting mobility number is reduced to ψ=32. From the temporal evolution of simulated bathymetry (Figure 6(b)), we observe organized sediment movement and small bedforms are generates at about t=100 sec (about 20 wave periods). The length of the ripple seems to be established first and then the ripples start to grow their height. At about t=300 sec (60 wave periods), the ripples reach their equilibrium length λ=0.46 m and height of η=0.078 m (ripple steepness η/λ=0.17). The simulated final ripple geometry is in very good agreement with ripple predictors of Wiberg and Harris (1994) and Mogridge et. al., (1994).

SedFoam is also capable of simulating reduction of ripple size via ripple splitting due to reduction of wave energy (reduction of wave orbital length). In Figure 7(a), we initialize the simulation with three large sand ripples (grain size d=0.44 mm) with length λ=0.46 m and height η=0.11 m (initial steepness η/λ=0.24 higher than realistic ripples). The oscillatory flow is driven by a simple harmonic wave motion of velocity amplitude U_0=0.48 m/s and wave period T=3 sec

(mobility number ψ=32). Due to a small wave period, the resulting ripple length and height are expected to be only λ=0.25 m and η=0.043 m (η/λ=0.17) according to the ripple predictor of Mogridge et. al., (1994). From the simulated temporal evolution of ripples shown in Figure 7(b), we can see that ripple height decays rapidly within the first 100 sec of simulation (33 wave periods). More importantly, to evolve into a smaller ripple length, ripple splitting occurs at an early stage into the simulation. By about t=150 sec (50 wave periods), it becomes evident that the domain contains 6 ripples as their height and length are slowly adjusting. The final ripple length and height in the simulation is λ=0.23 m and η=0.039 m, which agrees with ripple predictors. Without submodel extension for more sophisticated dilatancy and pore-pressure feedback effect, SedFoam is already capable of simulating ripple evolution and migration with good accuracy.

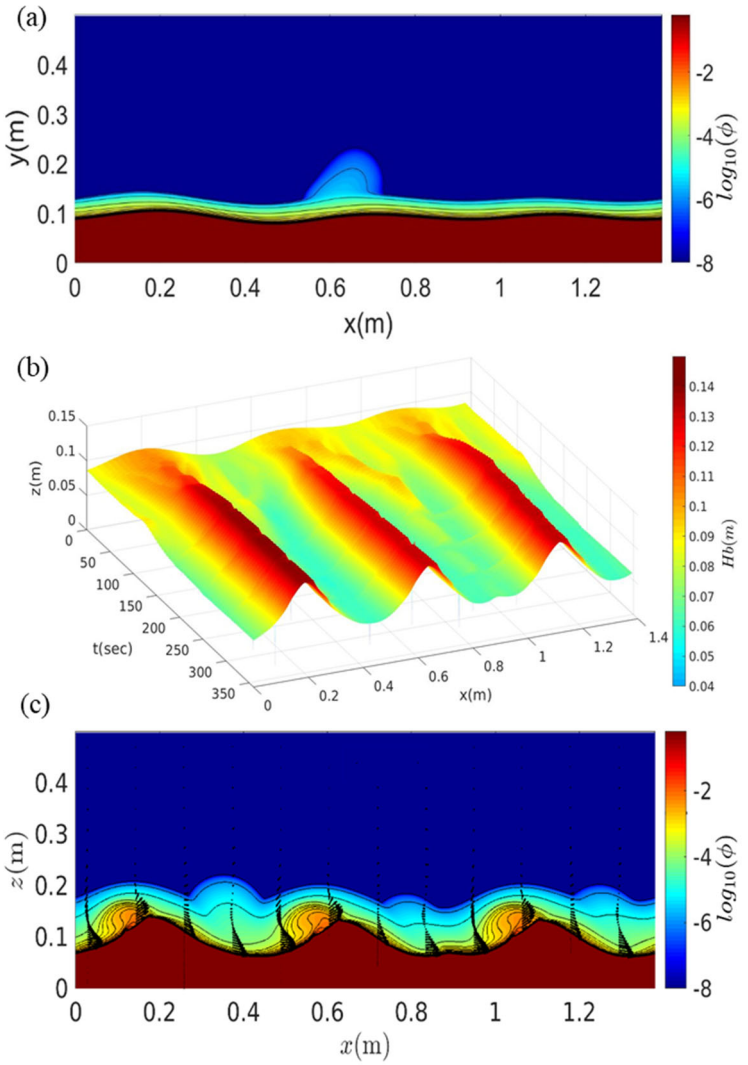

Figure 6: (a) Sediment concentration field of an energetic sheet flow (predominantly flatbed) used as initial condition. (b) Temporal evolution of bathymetry subject to a less energetic simple harmonic wave forcing. Predominantly flatbed evolves into three ripples. (c) Sediment concentration and velocity field at the end of simulation.

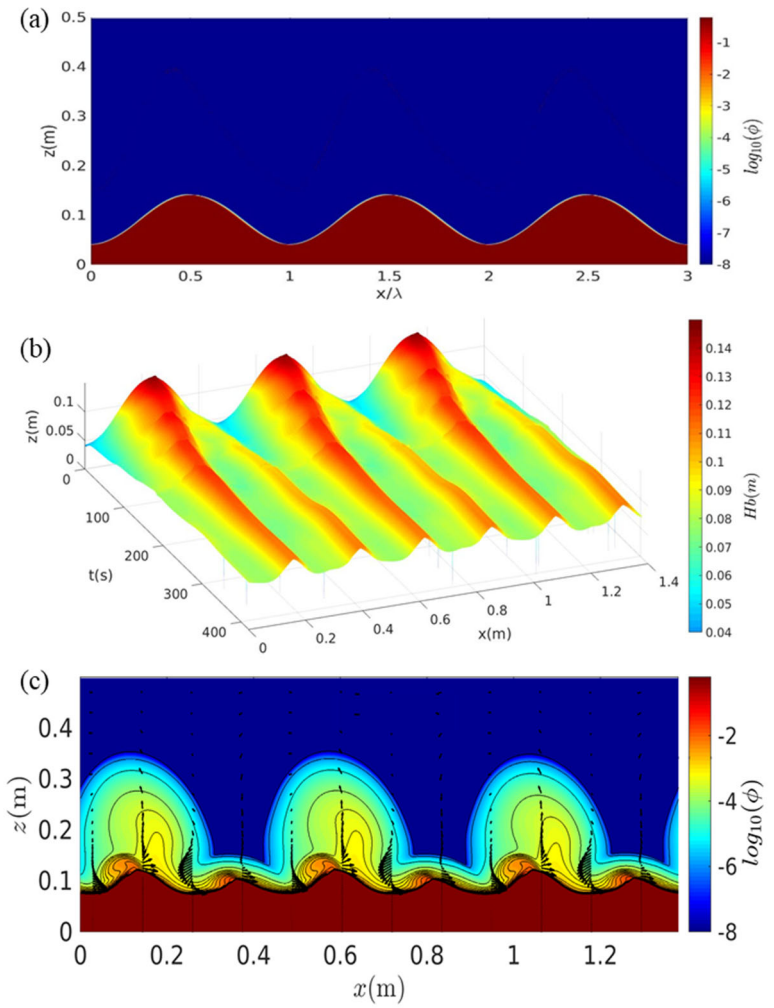

Figure 7: (a) Sediment concentration field used as initial condition. (b) Temporal evolution of bathymetry subject to a simple harmonic wave forcing of velocity amplitude U_0=0.48 m/s and wave period T=3 sec. Large bedforms evolve into six small ripples. (c) Sediment concentration and velocity field at the end of simulation.

4.3 Submodel for dilatancy and benchmark test for underwater avalanche (Task 2,3)

We propose a physical-based submodel for dilatancy, which is important to control the transition between fluid-like to solid-like behavior in the concentrated region of sediment transport. Dilatancy is the volume change of granular materials when subjected to shear deformation. This volume change, dilation or compaction, is due to rearrangement of micro-structure and it modifies the relationship between particle pressure (normal stress) and shear stress as particle concentration is below or above the critical state leading to the aforementioned fluid-like and solid-like behaviors. For sediment in water, this volume change can greatly modify pore pressure and further stabilize or destabilize soil. Dilatancy and its effect occur at sub-grid scale that cannot be directly resolved by the present Eulerian two-phase equations derived by averaging over individual grain and pore and therefore a sub-grid closure model is needed. The sub-model can be systematically described in three segments:

(1) Introducing dilatancy angle and its calculation:

Following an earlier model proposed by Pailha and Pouliquen (2009), a dilatancy angle is introduced to quantify the dilatancy effect and it is calculated as

$$\delta = K_1 \left(\phi - \phi_{eq}(I_v) \right) \tag{1}$$

where K_1=4 is an empirical coefficient and $\phi_{eq}(I_v)$ is the equilibrium volume concentration, which is calculated by mu(I) rheology following Boyer et al. (2011) in the viscous regime, or Chauchat (2018) for inertia regime. This equilibrium concentration can be considered as an estimation of critical state concentration. Dilatancy angle is further included in the calculation of particle pressure. In SedFoam, particle pressure is modeled as the summation of two components, the contact pressure P_c^P models the elastic behavior of sediment in very high concentration and the shear-induced pressure P_s^P describes the plastic behavior in moderate to high concentration. It is important to point out that because dilatancy occurs at the transition from plastic to elastic behavior, both components of particle pressure need to be revised in the following two steps.

(2) Dilatancy effect on contact pressure P_c^P:

The elastic behavior in SedFoam is modeled using Johnson and Jackson (1987) formulation for contact pressure. It has been modified to include dilatancy angle, written as

$$P_c^p = \begin{cases} 0 & \phi < \phi_{pl} \\ E \frac{[\phi - \phi_{pl}(\delta)]^3}{(\phi_{max} - \phi)^5} & \phi \geq \phi_{pl} \end{cases} \tag{2}$$

where E is an empirical granular bulk modulus. The plastic volume concentration ϕ_{pl}, which signifies a nominal concentration of plastic-elastic transition in equation (2), is calculated as a function of dilatancy angle. To account for the relaxation of volume concentration due to evolving dilatancy angle, ϕ_{pl} is calculated by integrating the following time-dependent equation:

$$\frac{d\phi_{pl}}{dt} = \phi_{pl} |\dot{\gamma}| \delta \tag{3}$$

where $|\dot{\gamma}|$ is the shear rate. The time integration of equation (3) renders a simple exponential function and hence the additional computational cost is minimum.

(3) Relaxation on shear induced pressure P_s^p:

Shear-induced pressure P_{sc}^p in SedFoam is currently calculated as part of the mu(I) rheology formulation in the viscous regime by following Boyer et al. (2011) or in the inertia regime by following Chauchat (2017). To better model the transition between plastic to elastic behavior, we also solve a relaxation equation for shear-induced pressure P_s^p:

$$\frac{dP_s^p}{dt} = \frac{1}{\tau_0} \left(P_{sc}^p - P_s^p \right) \tag{4}$$

The relaxation timescale is calculated as

$$\tau_0 = \frac{1}{K_2|\dot{\gamma}|\phi} \tag{5}$$

In this study, empirical coefficient K_2 is calibrated to be simply 1.0. The above formulation is inspired by Maxwell linear visco-elastic model so that transition from plastic to elastic behavior becomes more physically-based (Marzougui et al. 2015). The relaxation equation shown in equation (4) models the dynamic feature that a rapid flow (high shear rate) is accompanied by a short relaxation time where particles do not have time to move away from one another and resulting in a more elastic response (Rognon et al. 2011). On the contrary, a large relaxation time due to lower shear rate allows particles to adjust and separate from one another and hence shows more fluid/plastic behavior.

To evaluate the effect of dilatancy and pore-pressure feedback, SedFoam is benchmarked with a laboratory experiment of granular avalanche immersed in a high viscous liquid reported by Pailha et al. (2008). In this experiment, a granular bed (particle diameter d=0.16 mm, specific gravity 2.5) fully immersed in a water-oil mixture was prepared at different initial packing concentration (or porosity) for each run. The oil viscosity is $9.8 \times 10^{-6}\ m^2/s$. Granular avalanches were initiated by tilting the flume with an angle of 26.4 degree. The numerical model setup is essentially identical to that of the physical experiment (see Figure 8(a)). Particle velocity at the avalanche surface at the center of the flume, denoted here as avalanche velocity, is used for model-data comparison. From the comparison shown in Figure 8(b), it is very clear that SedFoam without dilatancy sub-model (SedFoam-O1) cannot reproduce the observed slow or rapid increase of avalanche velocity associated with the initially dense-packing or loose packing cases, respectively. In fact, without the dilatancy sub-model, SedFoam-O1 essentially predicted nearly identical linear increase of avalanche velocity regardless of initial packing concentration. On the other hand, once the appropriate dilatancy sub-model is included in the simulations (Figure 8(c)), SedFoam-O2 was able to reproduce the slow increase of avalanche velocity in dense condition (see gold curves with initial packing concentration 0.592), near linear increase of velocity in the critical state (red and blue curves at initial packing concentration around 0.58), and rapid increase of avalanche velocity in loose condition (magenta curves at initial packing concentration of 0.56~0.57). Generally, it is difficult to quantitatively compare pore pressure with a physical experiment as there usually exists, unavoidably, a small amount of air in the sand bed. Nevertheless, once the appropriate dilatancy sub-model is included, SedFoam-O2 is able to predict, at least qualitatively, the temporal evolution of pore pressure in the avalanche (see Figure 8(d)). As mentioned before, dilatancy represents the pore volume change when soil is subjected to shear which also causes the pore-pressure feedback. In the dense packing condition, external shear leads to dilation and generation of negative pore pressure (rapid drop in pore pressure from zero) due to suction of pore water. This feature is reproduced well by SedFoam-O2 (see gold curves in Figure 1d). In the loose packing condition, SedFoam-O2 is also able to reproduce the expected positive pore pressure (rapid increase of pore pressure from zero) due to expulsion of pore water during contraction (see magenta curves in Figure 8(d)). To achieve more quantitative agreement in pore pressure, it may require the consideration of slight compressibility of pore water due to a small amount of air content in the model. This model enhancement will be proposed as future work.

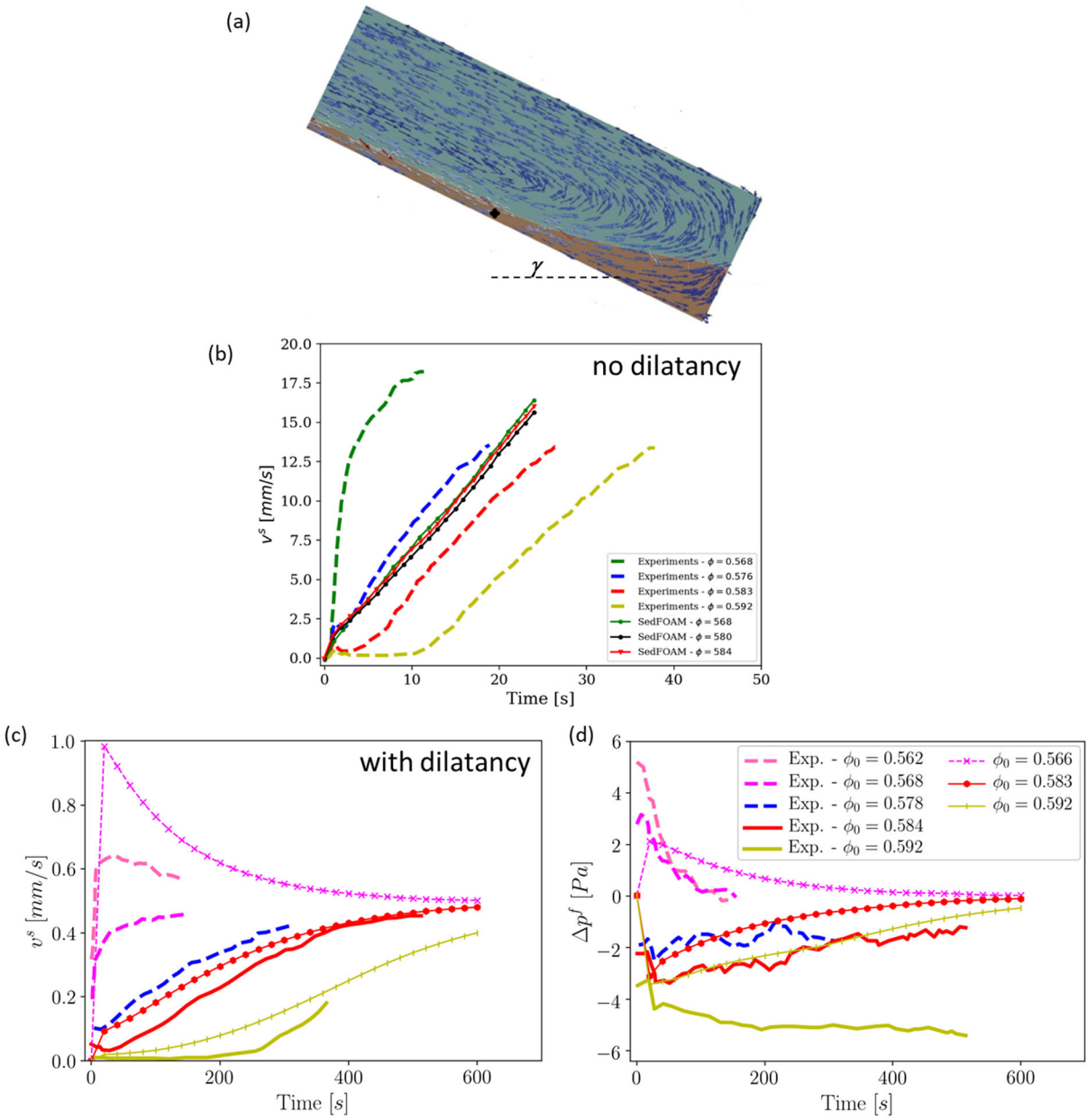

Figure 8: (a) A snapshot of underwater avalanche simulation. Temporal evolution of avalanche velocities for different initial concentrations calculated by SedFoam (b) without dilatancy and (c) with dilatancy submodel included. (d) Temporal evolution of excess pore pressure with dilatancy model included. Measure data is reported in Pailha et al. (2008).

4.4 Benchmark tests – piping (Task 3)

SedFoam-O1 is used to simulate laboratory experiments reported by Sumer et al. (2001). In this experiment, a circular pipe of diameter D=10 cm was placed on the sand bed (grain diameter d_{50}=0.18 mm and porosity *n*) with a small burial depth of e=0.64 cm (e/D=0.064). By adjusting the water level at the left-side of the pipe to be higher than that at the right-side, a horizontal pressure gradient is established in the experiment, which drives a seepage flow underneath the

pipe. We establish a 2D numerical model domain similar to the physical experiment, except that in order to save computational resources, we drive the pore water flow with a prescribed pressure distribution at the top boundary instead of adjusting the water level. From t/t_{liq}=0 to about t/t_{liq}=0.5, a weak seepage flow is driven underneath the pipe (from left to right), however, there is no notable change of sediment bed (see Figure 9(a)). As the seepage flow continues to propagate underneath the pipe and drives slow sediment movement, we observe the surface of the sand bed at the right side of the pipe starts to rise at t/t_{liq}=0.8 (see Figure 9(b)). At t/t_{liq}=1.0, the normalized horizontal pore pressure gradient exceeds 1.0 which triggers piping. Right after this moment, we observe rapid mobilization of sediment and at t/t_{liq}=1.09 (Figure 9(c)). A larger gap at the left side of the pipe can be clearly seen while the rise of the sand surface at the right side of the pipe becomes quite evident (also a very small gap but hard to see). Finally, in t/t_{liq}=1.12 (Figure 9(d)), mixture of sand and water is driven out and the pipe is completely detached from the sand bed with a gap of several millimeters. The subsequent erosion becomes very rapid and the scour depth increases rapidly (not shown). SedFoam-O1 is able to simulate the onset of scour via piping with main features that agree well with the laboratory observation (e.g., see Figure 5 of Sumer et al. (2001)).

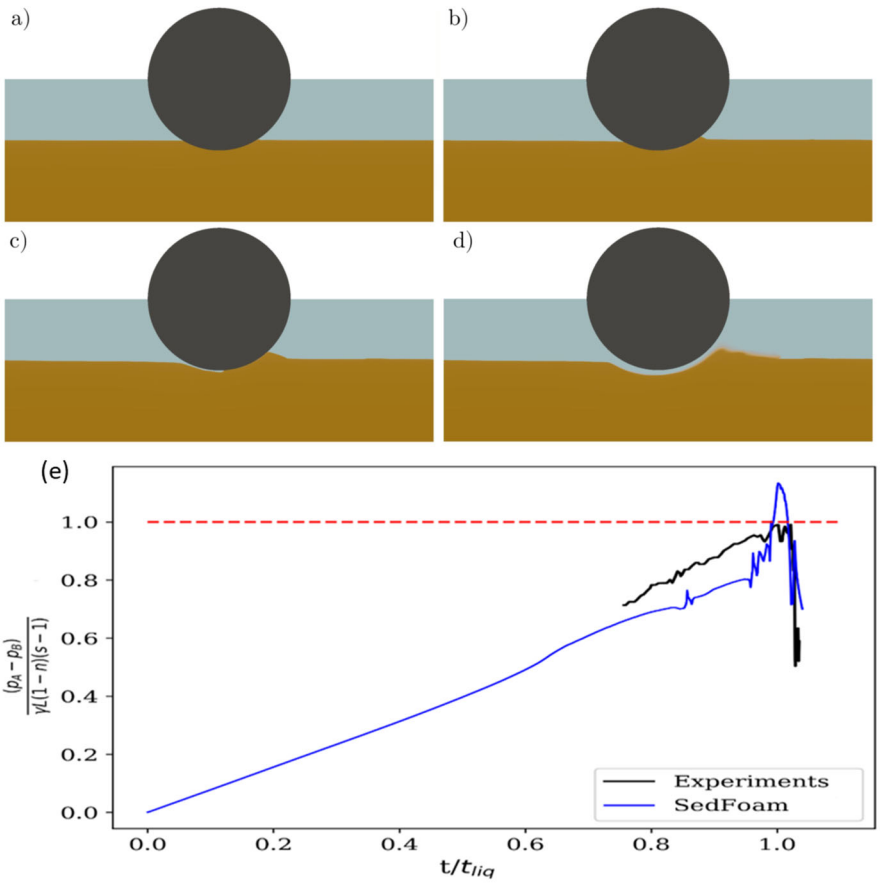

Figure 9: Snapshots of piping process simulated by SedFoam at (a) t/t_{liq}=0.5, (b) t/t_{liq}=0.8, (c) t/t_{liq}=1.09, (d) t/t_{liq}=1.12. Panel (e) shows the time series of normalized horizontal pore pressure gradient underneath the circular pipe between laboratory experiment and SedFoam-O1 results. Theoretically, piping occurs when normalized horizontal pressure gradient reaches 1.0 (red dashed line).

A more quantitative comparison of horizontal pore pressure gradient is shown in Figure 9(e). The evolution of pore pressure and their timing related to piping predicted by SedFoam-O1 are also similar to measured data. The only discrepancy is that SedFoam-O1 predicts normalized pore-pressure gradient exceeds unity and then decay, while measure data shows that the normalized pore-pressure gradient barely exceeds unity before the rapid decay. This discrepancy suggests that the pore-pressure predicted by SedFoam-O1 should dissipate faster as the sediment bed adjusts its micro-structure. This issue will be discussed next when a more complete dilatancy sub-model is incorporated. However, the fact that even with simple Option 1, SedFoam can reproduce main features in onset of scour due to piping is encouraging.

Although SedFoam-O1 without dilatancy sub-model can predict the key features of piping, numerical experiments suggest the piping simulation is not sensitive to the initial bed packing condition. In the original physical experiment of Sumer et al. (2001), although the author did not evaluate the effect of initial packing concentration in the bed, they did indicate that the experimental results presented were for relatively loosely-packed beds. This implies that the physical process of piping should at least weakly depending on initial packing concentration. By including the dilatancy submodel discussed in Section 4.3, SedFoam is able to predict the earlier occurrence of piping when initial packing concentration in the bed is smaller. Figure 10 shows the time series of normalized pore pressure difference for a case without dilatancy model (dashed line) and three cases with the new dilatancy model incorporated but with different initial sediment bed concentration. The red dashed line with normalized pore pressure difference equals to unity represents the criteria for piping. As we have pointed out previously, results without including the dilatancy model show a large overshoot of pressure difference by about 25%. Once the dilatancy model is included, the overshoot decreases. More importantly, the model results with dilatancy model included show sensitivity to initial bed condition. For instance, when the initial packing in the sediment bed is looser, the occurrence of piping is earlier. These are expected behaviors in soil mechanics. Figure 11 shows more clear evidence that the dilatancy effect plays an important role in piping. According to the distribution of dilatancy angle in the sediment bed, we can see that at t=60 sec (before piping occurs) the dilatancy angle just underneath the pipe is of negative value, which indicates a contraction behavior due to initial loose packing (initial sediment concentration is smaller than critical state concentration). Contraction of granular skeleton causes reduction of pore space and pore water must be expelled from the pore space. The outcome of this microstructure rearrangement is parameterized as reduction of friction, which leads to earlier occurrence of piping and faster relief of pore pressure. This piping benchmark test is encouraging as it provides evidence that the new dilatancy sub-model, originally calibrated with underwater avalanches, is also effective for other applications.

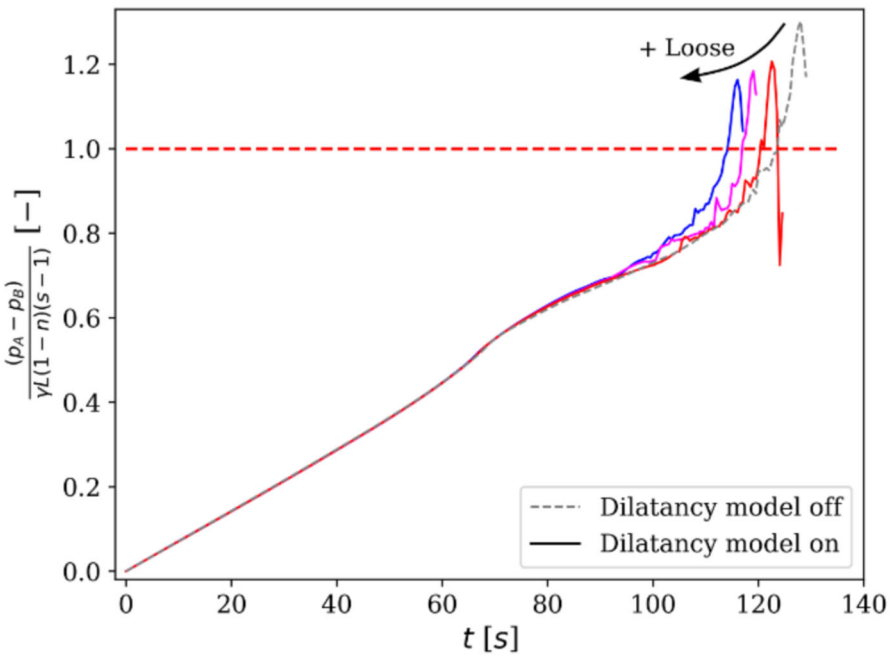

Figure 10: time series of pressure gradient underneath the 2D pipeline for model runs without (dash line) and with dilatancy sub-model (solid lines; different colors represent results of different initial bed concentration).

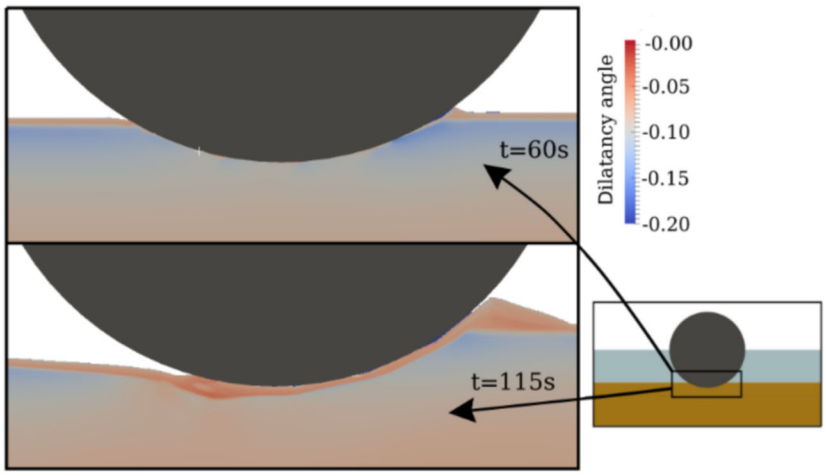

Figure 11: Snapshots of spatial distribution of dilatancy angle in the sand bed underneath the 2D pipeline. Negative dilatancy angle represents contraction (reduction of friction).

4.5 Scour of a 3D short cylinder in high KC number at field scale (Task 4)

As mentioned before, evaluating SedFoam's capability to simulate the scour of a 3D short horizontal cylinder is a vital part of this proof-of-concept project as the future simulations of UXO can be simplified into horizontal short cylinder configuration as it consists of all the essential 3D features. Including the simulation presented in Section 4.1, we have carried out three simulations for scour around a 3D short cylinder each with different KC number and Shields parameter. These simulations are similar to the cases presented in the laboratory experiment of Dimer and Garcia (2007). In Section 4.1, we have presented the model result for a case of the lowest KC number and Shields parameter (Case 1: KC=4.8, θ=0.05) as part of Task 1 to set up the optimum domain for 3D scour problem. In this section, we focus on two other cases with more energetic wave conditions (Case 2 and Case 3), and these wave conditions are similar to the range of intensity observed at Duck, NC reported by Klammler et al. (2019). In these two cases, the cylinder is of diameter D=8.6 cm and length L=34.4 cm. The model domain setup and mesh are similar to that shown in Figure 2. The cylinder is placed over the sand bed consisting of sand with grain diameter 0.25 mm and the initial burial depth is e=0.258 cm (e/D=0.03). For the moderate wave condition Case 2, the wave period is T=6 sec and orbital velocity amplitude is 0.4 m/s, which gives KC=27.9 and θ=0.155. For the high wave energy condition Case 3, the orbital velocity amplitude is 0.8 m/s, which gives KC=55.8 and θ=0.541. For the Shields parameter as large as θ=0.541, sediment transport mode is approaching the sheet flow condition even without the presence of a cylinder.

Figure 12(a) shows a snapshot of the velocity field at the center plane, streamlines, coherent structures and bathymetry at the very early stage of the simulation (wave crest of the first period) for Case 2 (KC=27.9; θ=0.155). It is evident that as the intense flow goes over the cylinder, the incoming boundary layer flow separates at about 4 cm in front of the cylinder due to adverse pressure gradient imposed by the presence of the cylinder (Figure 12(a)). The main signature due to this boundary layer separation is the generation of horseshoe vortex immediately downstream, which can be clearly identified by the streamline pattern and coherent structure contour close to the cylinder near the bed. The generation of horseshoe vortex for vertical piles is well-documented (Roulund et al. 2005). For a 3D short cylinder shown here, we observe that during the initial stage, due to the blocking of the short cylinder, horseshoe vortex can also be generated at the stoss side. Based on the streamline pattern, the horseshoe vortex extends to the two lateral faces of the cylinder where flow speed is enhanced and leading to more significant local scour. In the subsequent wave trough interval (Figure 12(b)), flow reverses direction and now this side of the cylinder becomes the lee-side and flow separation (lee-wake) can be observed. Due to the oscillatory flow, a given side of the 3D short cylinder experiences horseshoe vortices and lee-wake flow structure which drive the scour process. At the later stage (Figure 13(a)) during the trough period of the 5^{th} wave, the lee-wake flow structures become more pronounced. On the contrary, shown in Figure 13(b), for the subsequent crest period of the 6^{th} wave, the horseshoe vortex is not visible at the stoss side of the cylinder because scour underneath the cylinder has broken through the sediment bed in several spots and the overall adverse pressure gradient becomes too weak to cause significant boundary layer separation of the incoming flow. However, the flow on two lateral faces of the cylinder remains strong and more scour continues (see later discussion on Figure 15(a)).

Figure 14 shows snapshots of the velocity field at the center plane, streamlines, coherent structures and bathymetry for Case 3 with high KC=55.8 8. Due to more intense oscillatory flow in this highest KC number run, horseshoe vortex and strong lateral flow pattern can be more clearly seen (Figure 14(a)). In fact, the flow is so intense and the estimated Shields parameter is θ=0.541, which is near the sheet flow condition. Therefore, simply approaching the 2nd wave period, simulation results suggest that most of the sediment underneath the cylinder has been eroded and hence horseshoe vortex is no longer observed at the second wave cycle (Figure 14(b)).

Figure 15 summarized the scour bathymetry at three different cross-sections for Case 2 (Figure 15(a)) and Case 3 (Figure 15(b)). For Case 2 with medium KC number (θ=0.155), after the waves persist for 6 wave cycle (t=25.5 sec), more significant scour depth up to 0.06 D (5~6 mm) is observed at two lateral faces of the cylinder (y=-2.0 and 2.0D). However, the sediment bed is still connected to the cylinder near its central portion. On the other hand, for Case 3 (Figure 15(b)) with high KC number (θ=0.541), very large and asymmetric scour depths are observed at two lateral faces of the cylinder just at the end of the first wave cycle. The scour depth at the right side of the cylinder (y=-2.4D) is larger and reaches 0.17D (15 mm). Near the central plane of the cylinder (y=0.0 D), the cylinder remains attached to the bed. At this stage in reality, the 3D cylinder should tilt to the right side of the scour hole and cause a more asymmetric scour pattern, as described in the laboratory experiment of Dimer and Garcia (2007).

In summary, we have successfully carried out high KC number and Shield parameter simulations on scour of 3D short cylinder driven by oscillatory flow similar to field observation at Duck, NC. Interesting flow patterns such as horseshoe vortices at the earlier stage, flow acceleration at two lateral faces of the cylinder and lee-wake flow structure have been predicted by the model. Moreover, model results show much significant scour at two lateral faces of the cylinder that is consistent with laboratory measurement by Dimer and Garcia (2007), which further causes subsequent tilting of the cylinder. In the highest KC number case with Shields parameter approaching sheet flow condition, significant scour up to 15 mm at one lateral face of the cylinder is obtained in just one wave period, which will cause cylinder tilting. In the future, it is important to expand SedFoam for simulating moving object capability in order to further predict the scour burial process.

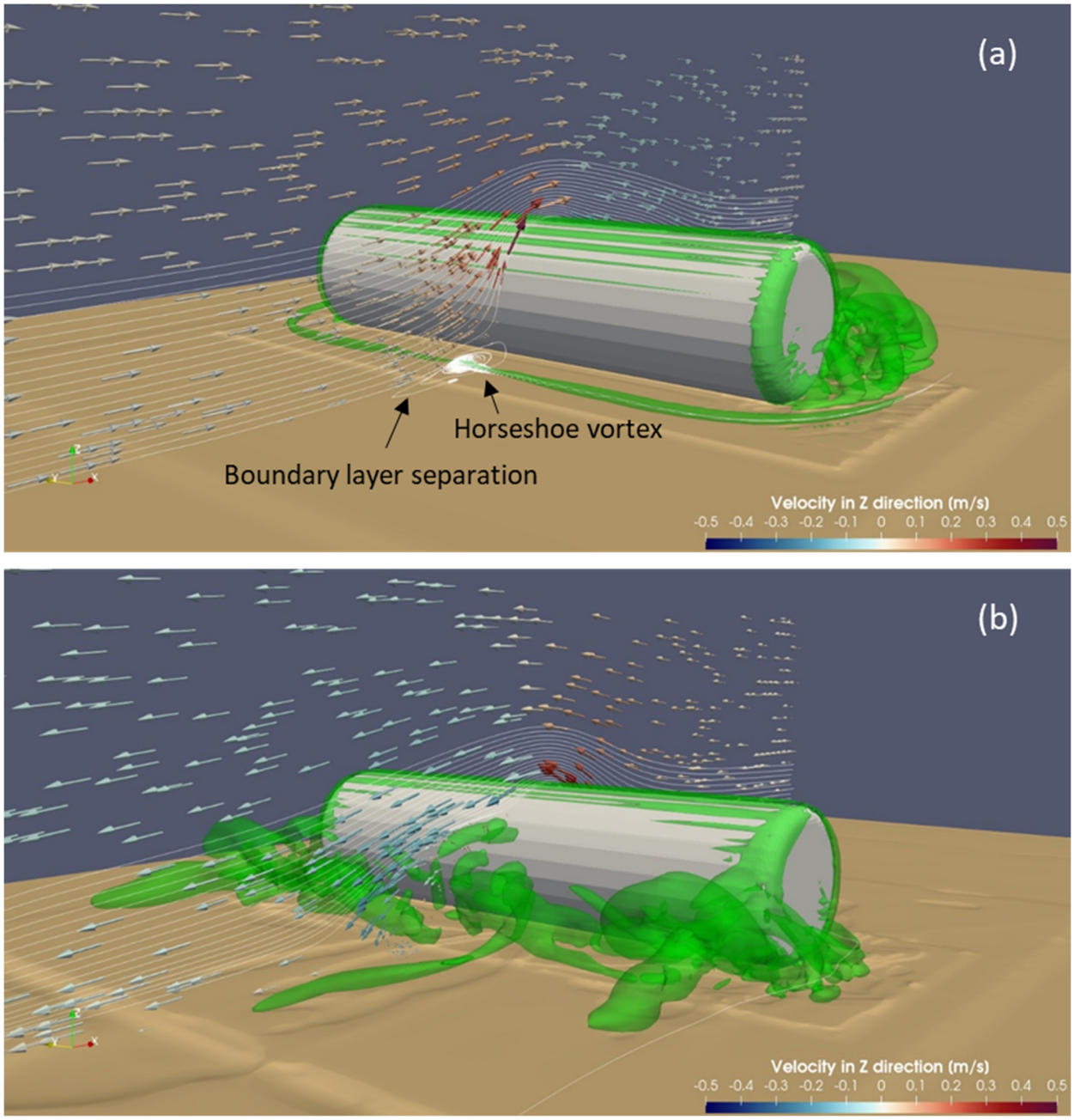

Figure 12: Scour of a 3D short cylinder for Case 2 with medium KC=27.9 at the initial stage. (a) A snapshot of velocity field, streamlines, coherent structures and bathymetry at wave crest of the 1st period and (b) a snapshot at the wave trough of the 1st period. The color (see color bar) on the velocity vectors represent the vertical component of the velocity. The coherent structures are identified using iso-surface of vortex vector with magnitude |R|=15 (1/s).

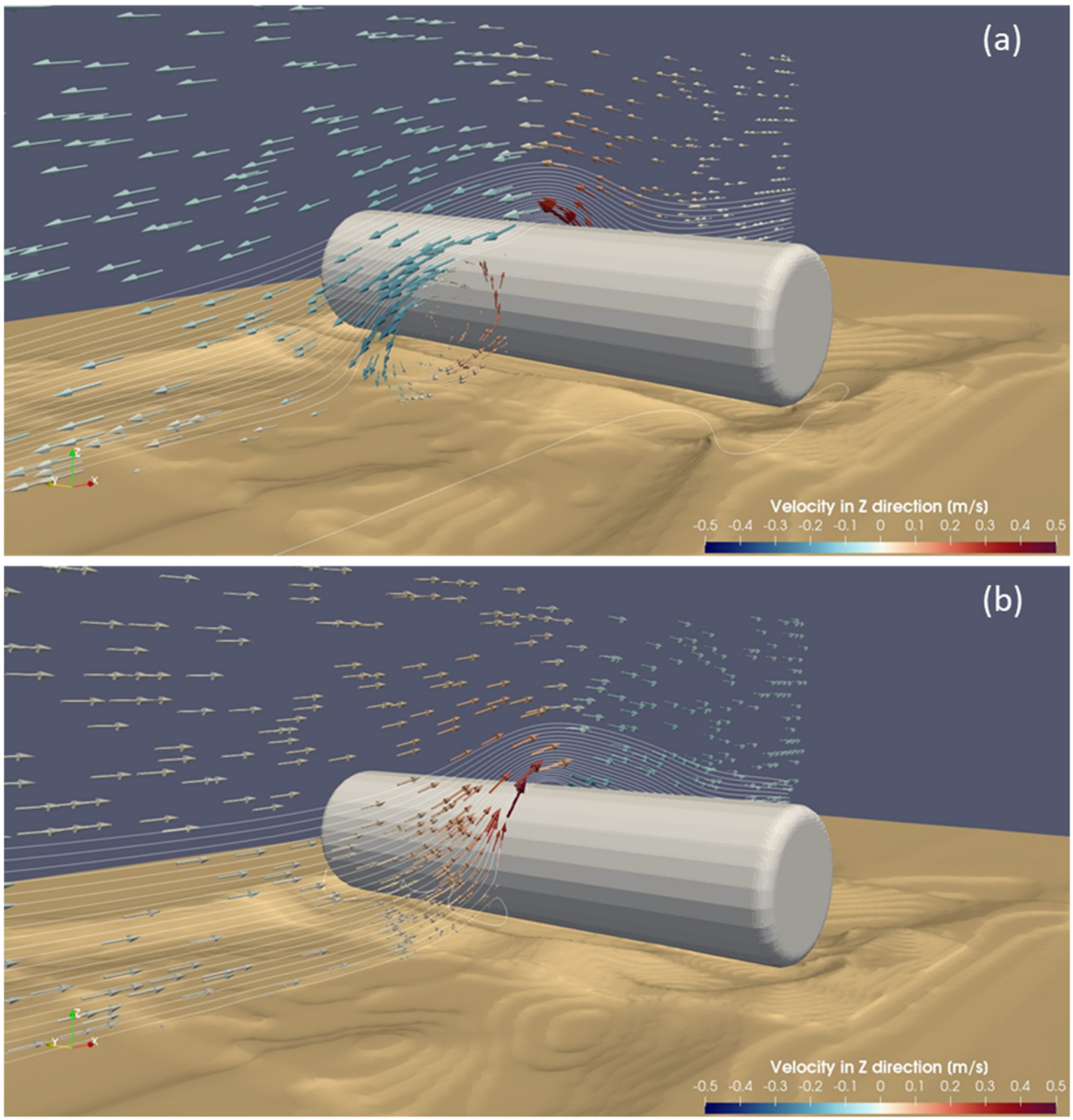

Figure 13: Scour of a 3D short cylinder for Case 2 with medium KC=27.9 at later stage. (a) A snapshot of velocity field, streamlines, and bathymetry at wave trough of the 5th period and (b) a snapshot at the wave crest of the 6th period. The color (see color bar) on the velocity vectors represent the vertical component of the velocity. Coherent structure is removed to better observe the scoured bathymetry.

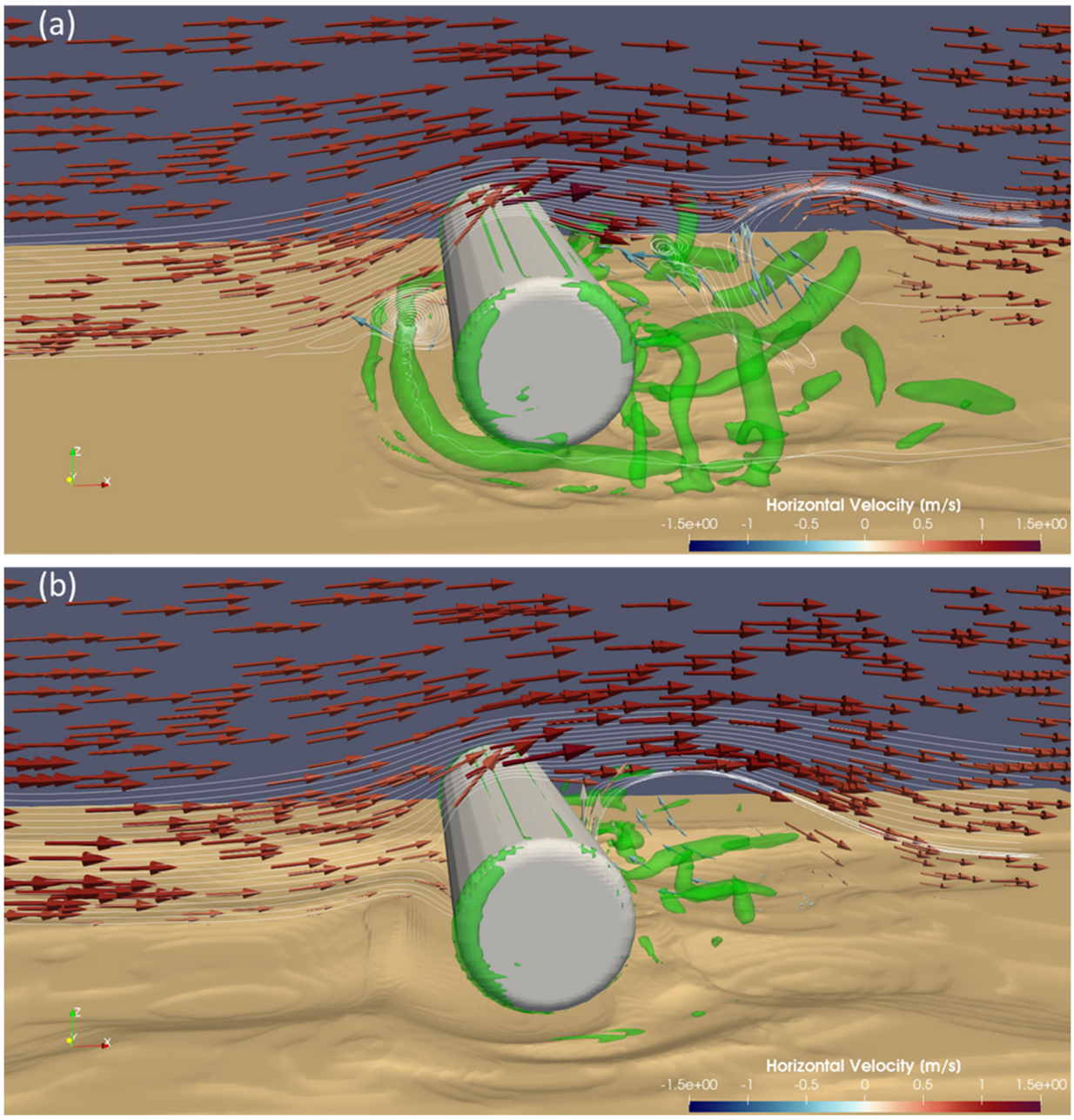

Figure 14: Scour of a 3D short cylinder for Case 3 with high KC=55.8. (a) A snapshot of velocity field, streamlines, coherent structures and bathymetry at the beginning of the 1st period and (b) a snapshot during acceleration to the wave crest of the 2nd period. The color (see color bar) on the velocity vectors represent the vertical component of the velocity. The coherent structures are identified using iso-surface of vortex vector with magnitude |R|=25 (1/s).

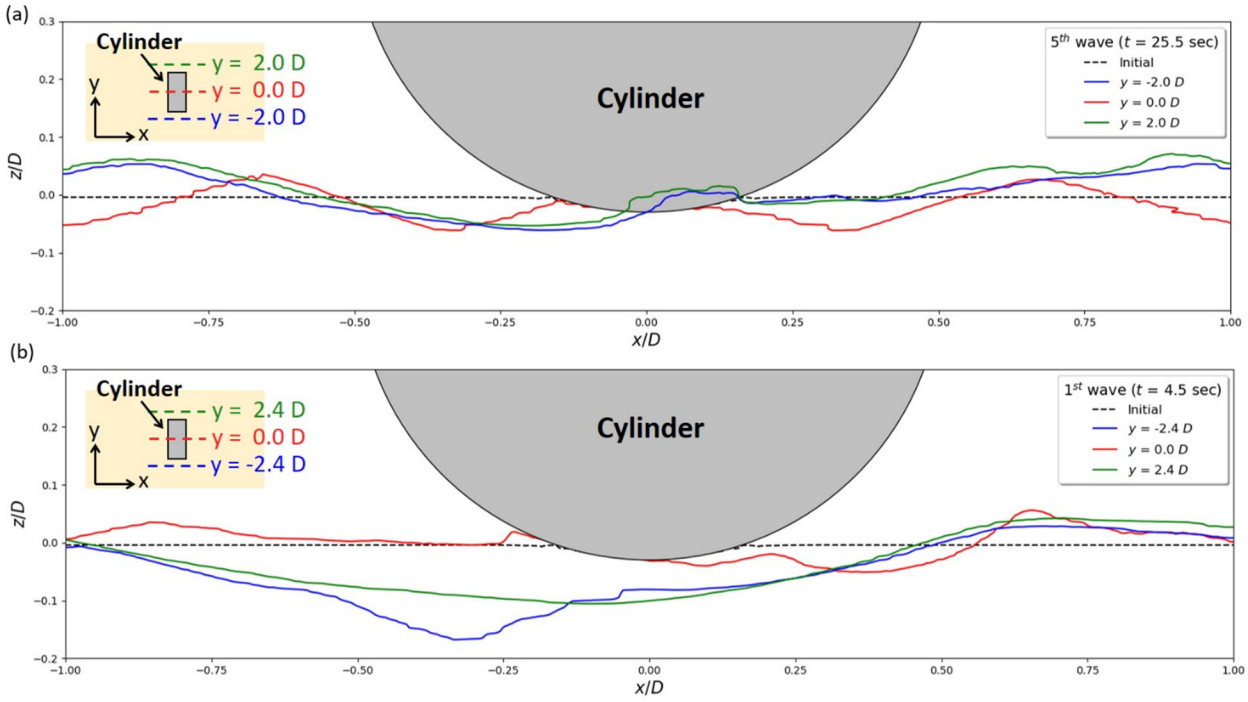

Figure 15: Side views of the bathymetry to illustrate the scour pattern for (a) medium KC=27.9 Case 2 at three difference cross-section (y=-2.0D, 0.0D and 2.0D) at the beginning of the 6th wave period (t=25.5 s); (b) High KC=55.8 Case 3 at three difference cross-section (y=-2.4D, 0.0D and 2.4D) near the end of 1st wave period (t=4.5 sec).

4.6 Scour of an initially slightly-buried object and backfill process (Task 4)

In typical single-phase scour models, the object cannot be directly attached or buried into the sand bed and a small gap has to be artificially introduced. When an object is settled on the seabed in reality, it is always attached and more often slightly buried in the seabed and the onset of scour is mainly due to pore water (seepage) flow passing underneath the object caused by pressure difference between upstream and downstream of the object. In Section 4.4, the two-phase model SedFoam is used to simulate a laboratory experiment reported by Sumer et al. (2001) for onset of scour, or called piping, of a slightly buried 2D fixed pipeline driven by a prescribed pressure difference between two sides of the pipe. This demonstration is very important because it demonstrates one of the main reasons to pursue a two-phase modeling methodology, that is, to allow more realistic interaction between the soil response, sediment transport and the objects.

As the first proof-of-concept simulation, we carry out numerical investigation on a fixed pipeline scour driven by oscillatory flows with a small initial burial depth. The pipeline is of diameter D=10 cm and it is fixed over a sand bed with a small initial burial depth of e=0.64 cm (e/D=0.064). The sand bed consists of grain diameter d_{50}=0.18 mm. The oscillatory flow has a period of T=4 sec and it takes about 4 wave periods for the flow intensity to reach the target velocity amplitude of 0.45 m/s. It is clear that for the first few wave periods, no scour is developed (see Figure 16 at t=11

sec). The interaction between the boundary layer flow and the pipeline causes local flow acceleration and flow separation, which lead to several minor sediment erosion spots (e.g., see x=0.14 m) but they occur quite away from the pipeline. Moreover, we observe in Figure 16(c) that as the main flow is directed to the offshore direction (left) in wave trough period and causes flow separation on the offshore side of the pipeline, the excess pore pressure in the sediment bed also decreases toward the offshore side of the pipeline (from about +30 to -30 Pa). However, this pressure difference is relatively small and it drives a rather small seepage flow toward the offshore side of the pipeline. During the passage of wave trough of the 5^{th} wave (see Figure 17 at t=18 sec), we observe a much intense boundary layer flow passing over the cylinder toward the offshore direction and a stronger flow separation at the offshore side of the pipeline is observed (see Figure 17(b),(c)). At this moment, the pore pressure difference between the onshore and offshore side of the pipeline becomes much stronger (from about +150 to -150 Pa), which drives larger seepage flow underneath the pipeline. The normalized pore-pressure gradient is seen to just exceed the threshold value of 1.0 (see Figure 17(a)). Only 0.3 sec later (see Figure 18), we observe notable erosion and tunneling just under the onshore side of the pipeline (see the white box in Figure 18(b)). This small gap allows incoming flow to enter the narrow space underneath the pipeline and more erosion has occurred. Another 0.4 sec later (see Figure 19), the piping process has been completed and the fixed pipeline is fully detached from the sediment bed. The small gap allows high speed flow to pass through and causes more significant erosion. By t=60 sec (Figure 20), a 2 cm gap can be clearly seen between the fixed pipeline and the scoured sediment bed. These features observed in the present simulation are very similar to those described in the laboratory observation by Sumer et al. (2001) carried out in a wave flume.

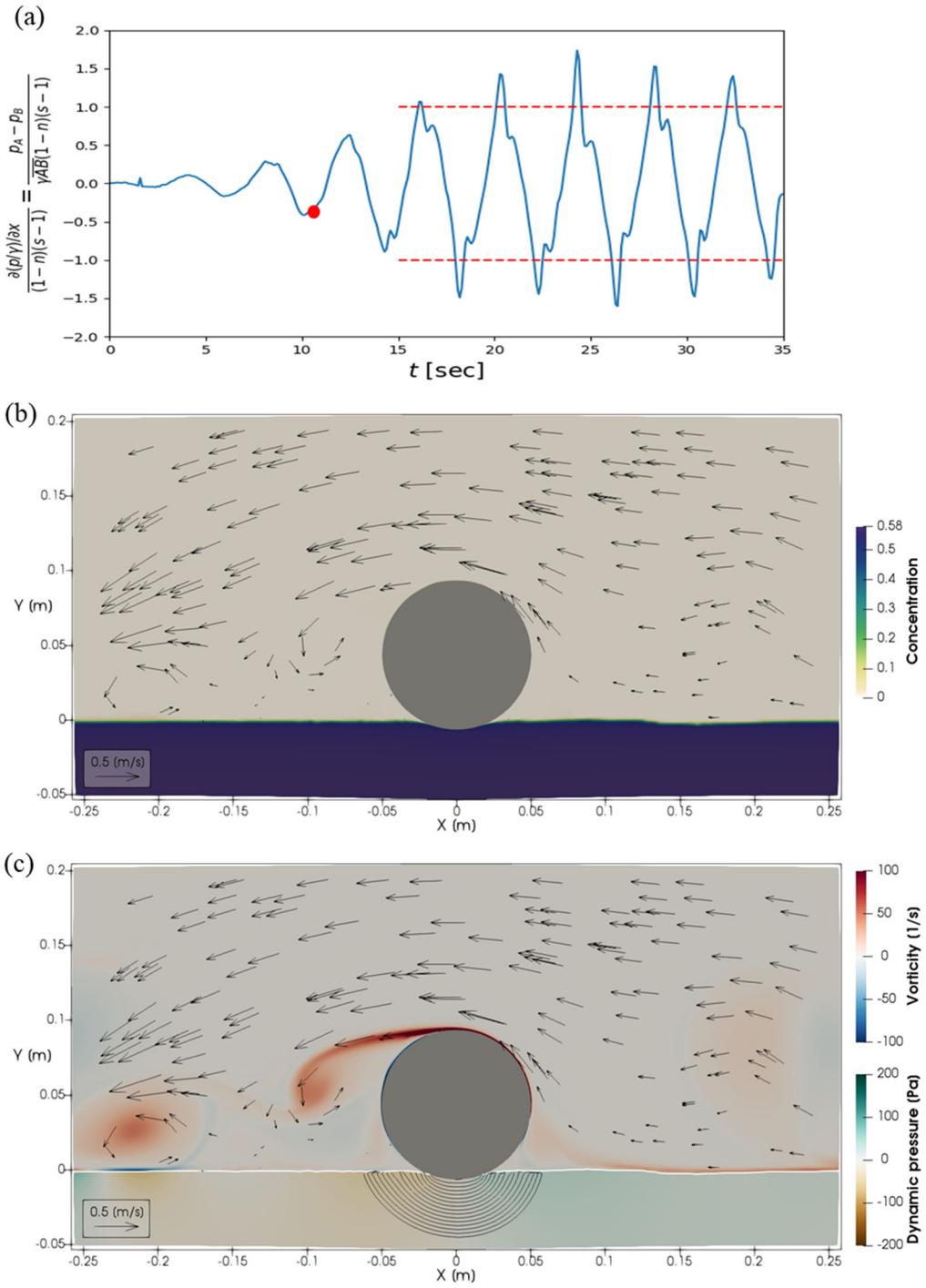

Figure 16: Scour of a 2D pipeline driven by oscillatory flow with realistic onset due to piping at t=11 sec. (a) time series of pressure difference immediately upstream and downstream of the pipe. Panel (b) shows a snapshot of sediment concentration field and velocity vectors while panel (c) shows the corresponding vorticity field and dynamic pore pressure in the sand bed. The lines in the sediment bed show streamlines of the seepage flow.

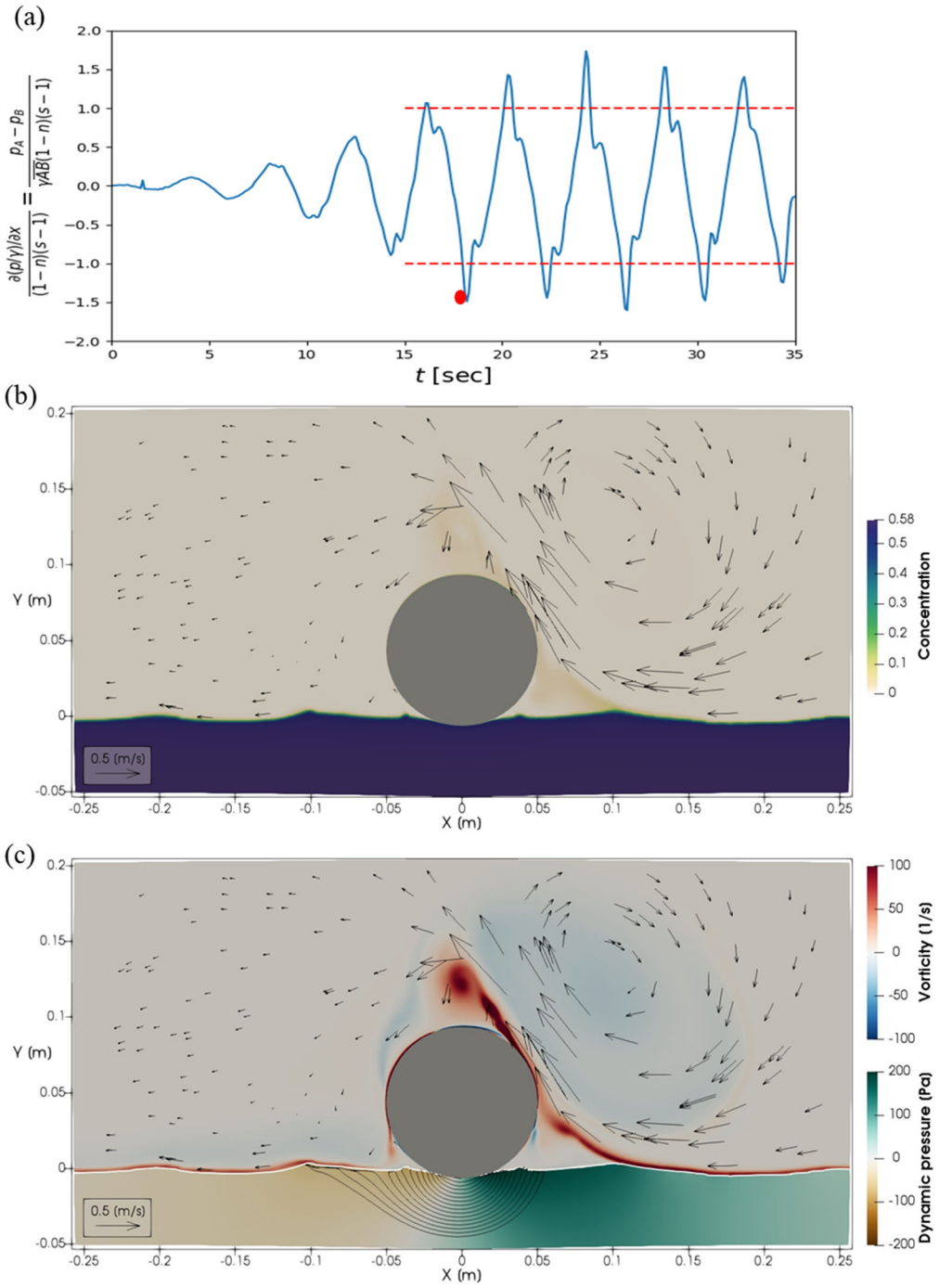

Figure 17: Scour of a 2D pipeline driven by oscillatory flow with realistic onset due to piping at t=18 sec. (a) time series of pressure difference immediately upstream and downstream of the pipe. Panel (b) shows a snapshot of sediment concentration field and velocity vectors while panel (c) shows the corresponding vorticity field and dynamic pore pressure in the sand bed. The lines in the sediment bed show streamlines of the seepage flow.

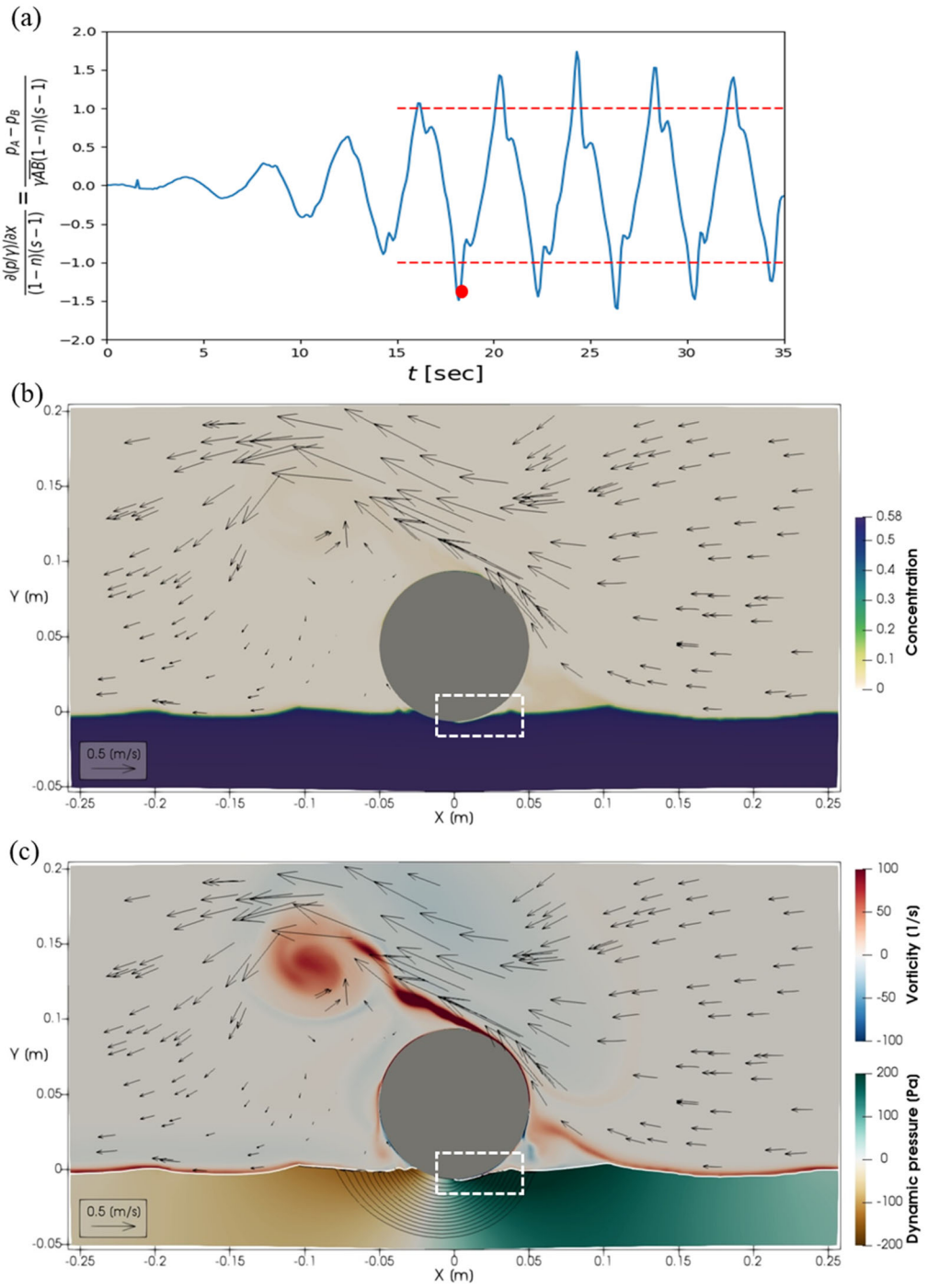

Figure 18: Scour of a 2D pipeline driven by oscillatory flow with realistic onset due to piping at t=18.3 sec. (a) time series of pressure difference immediately upstream and downstream of the pipe. Panel (b) shows a snapshot of sediment concentration field and velocity vectors while panel (c) shows the corresponding vorticity field and dynamic pore pressure in the sand bed. The lines in the sediment bed show streamlines of the seepage flow.

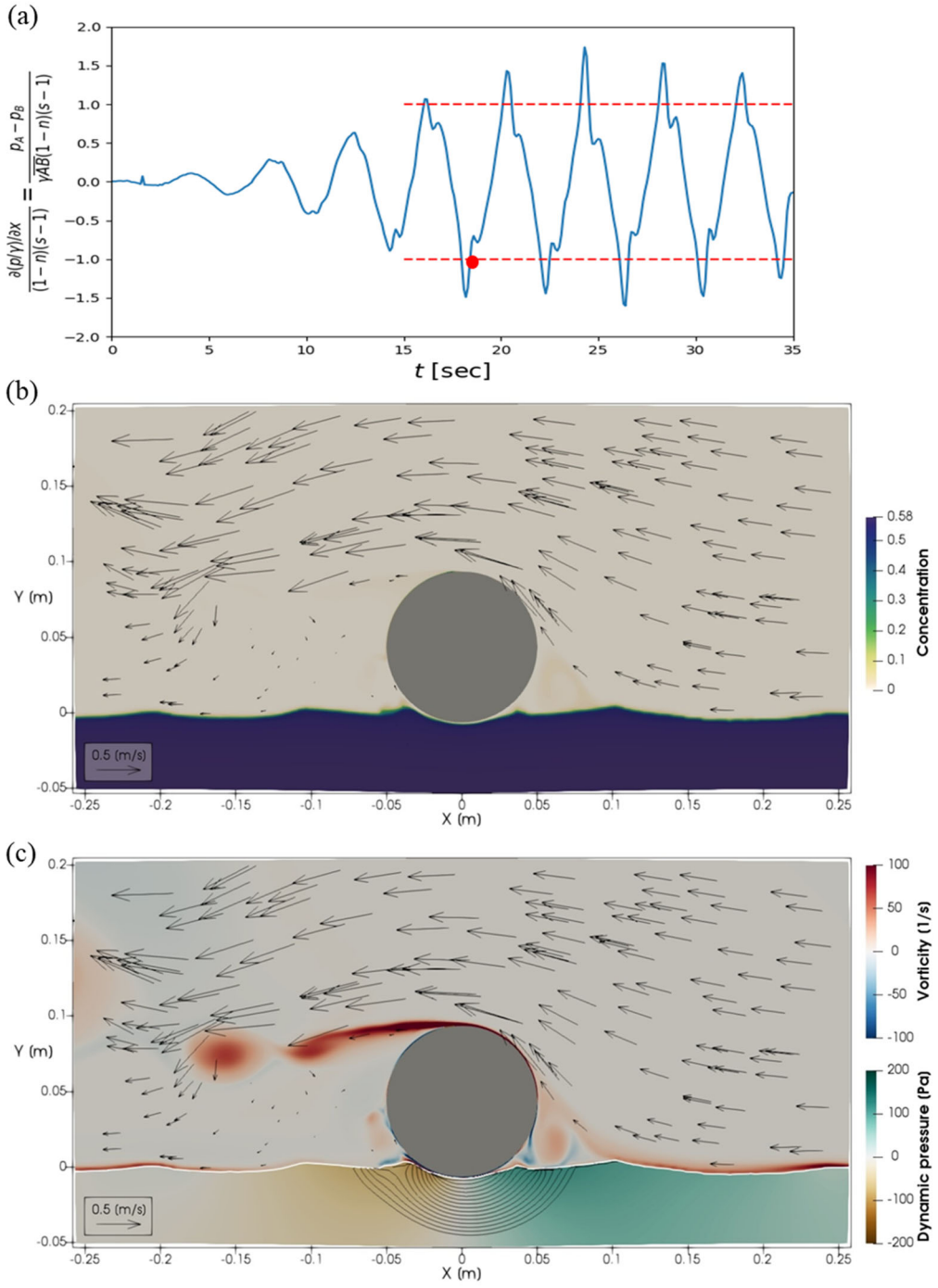

Figure 19: Scour of a 2D pipeline driven by oscillatory flow with realistic onset due to piping at t=18.7 sec. (a) time series of pressure difference immediately upstream and downstream of the pipe. Panel (b) shows a snapshot of sediment concentration field and velocity vectors while panel (c) shows the corresponding vorticity field and dynamic pore pressure in the sand bed. The lines in the sediment bed show streamlines of the seepage flow.

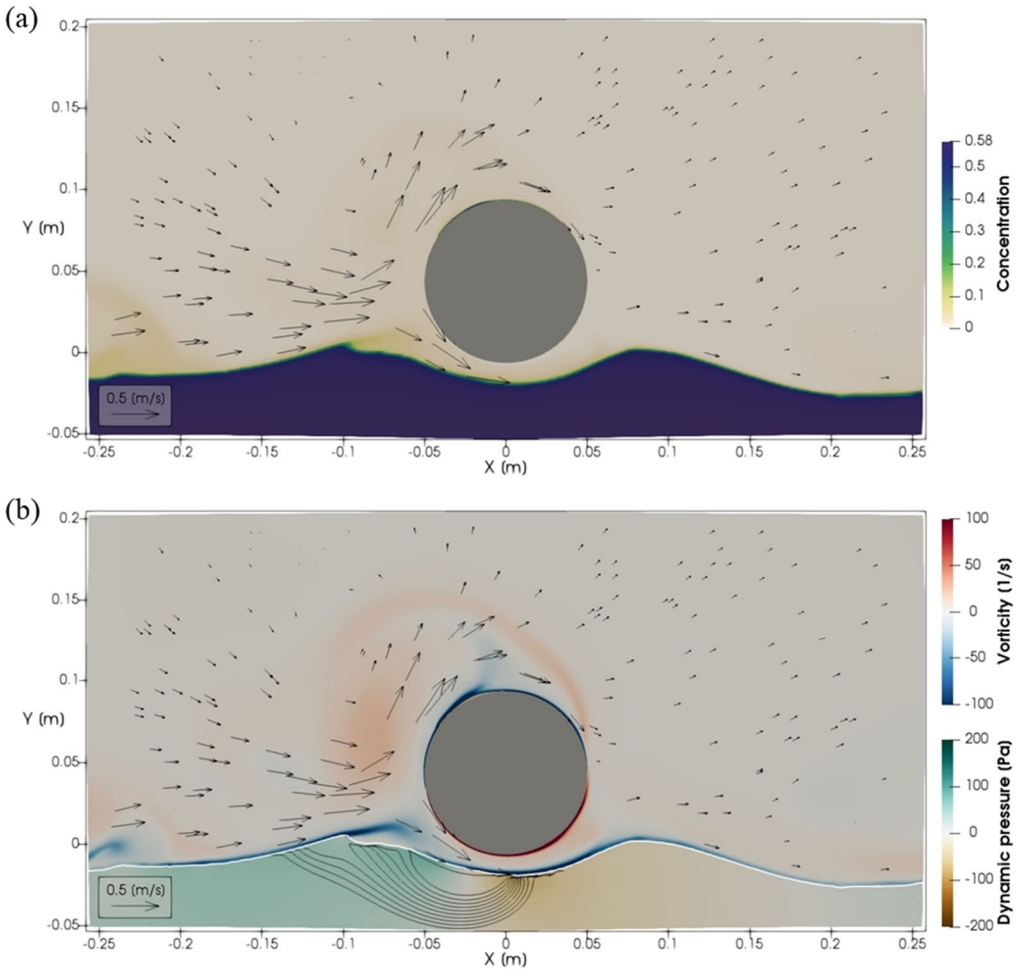

Figure 20: Scour of a 2D pipeline driven by oscillatory flow with realistic onset due to piping at t=60 sec. Panel (a) shows a snapshot of sediment concentration field and velocity vectors while panel (b) shows the corresponding vorticity field and dynamic pore pressure in the sand bed. The lines in the sediment bed show streamlines of the seepage flow.

In the next numerical investigation, we use the sand bed obtained at t=60 sec (Figure 20) as the initial condition for the sediment phase. However, the pipeline is moved downward so that it is attached to the sediment bed and effectively buried into the sand bed by about 1/3 of the pipeline diameter (see Figure 21(a)). Because 1/3 of the pipeline is now sheltered by the sand bed, the perturbations introduced by the pipeline and the bathymetry start to encourage a minor burial. In Figure 21(b), we can clearly observe that the primary vortex induced by flow separation at the right (onshore) side of the pipeline during crest flow drives a strong return flow near the sand bed. This return flow effectively erodes and transports sediment toward the pipeline and causes more burial. At later time in t=33 sec (Figure 21(c)), the pipeline is about half-buried into the sand bed.

Compared to Figure 21(d) at t=48 sec, the burial depth is about the same and we can see that the burial process has more or less approached an equilibrium state.

SedFoam's capability to simulate more realistic onset of scour via piping driven by an oscillatory flow and the subsequent burial processes has been demonstrated in this project. What is needed now is to implement the capability of moving the object following a force balance and the equation of motion in order to carry out full simulations of scour burial processes.

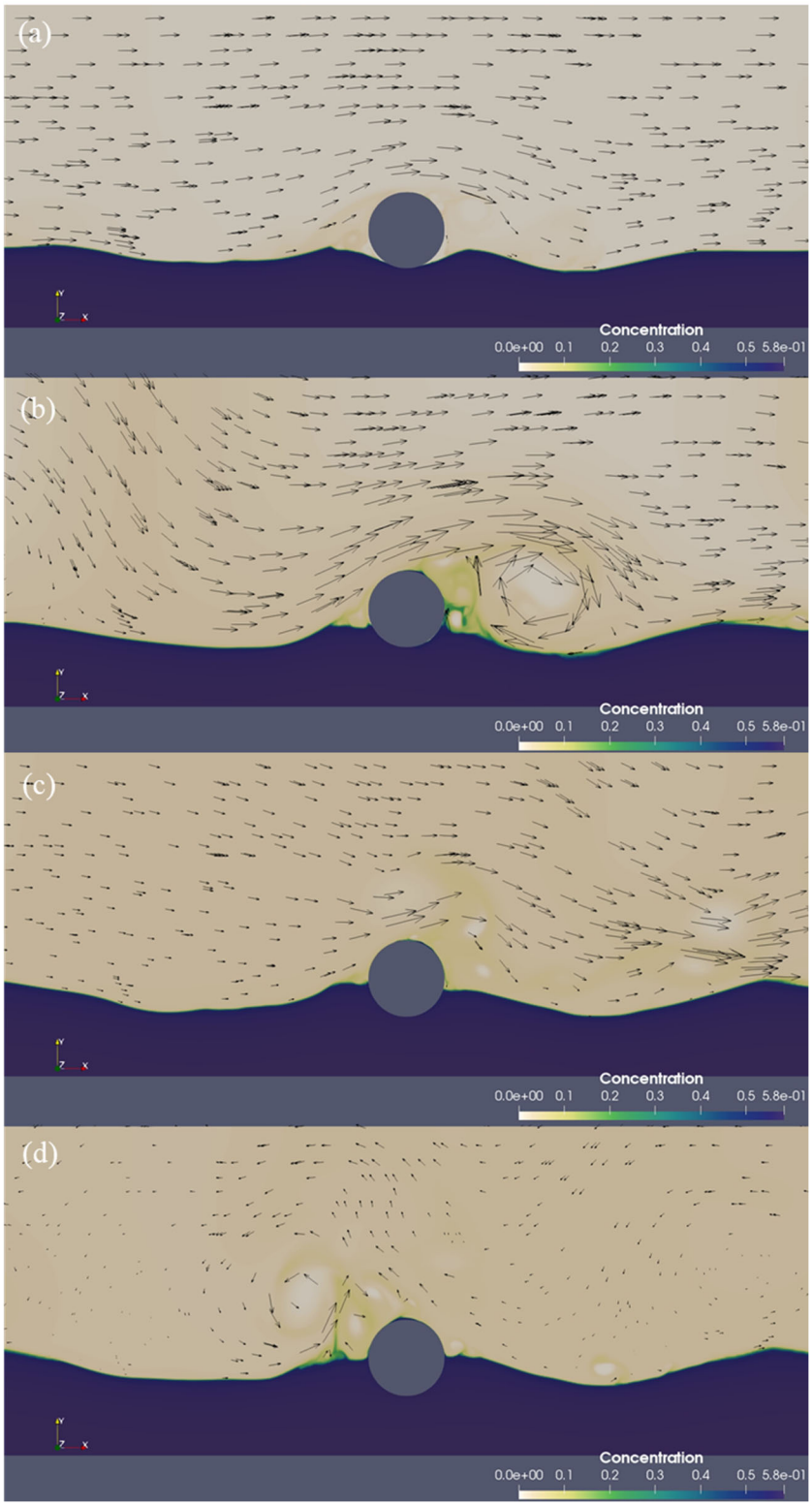

Figure 21: Backfill of a partially buried 2D pipeline. (a), (b), (c) and (d) show snapshots of sediment concentration field and velocity vectors at t=1.0, 17.0, 33.0 and 48.0 sec, respectively.

4.7 Ripple migration driven by skewed and asymmetry waves (Task 4)

Bedforms are ubiquitous in coastal environments. The evolution and migration of bedforms can also cause burial and reemergence of UXOs. Modeling sediment transport via bedform migration and its interaction has been a challenging task in single-phase CFD models (e.g., Chou and Fringer 2010). In this study based on a two-phase modeling framework, we also investigate SedFoam's capability to simulate migration and evolution of bedforms driven by waves. In Section 4.2, we demonstrate SedFoam's capability to simulate evolution of ripple geometry subject to changing intensity of sinusoidal waves without net migration. The simulated bedform geometries agree very well with empirical ripple predictors. In this section, we further discuss our proof-of-concept numerical investigation on SedFoam's capability in simulating ripple migration subject to typically encountered nearshore nonlinear waves with onshore-directed velocity skewness (for typical shoaling waves before breaking) and acceleration skewness (typical breaking waves with steep wave fronts).

We first present SedFoam's simulation of onshore ripple migration driven by onshore-skewed velocity similar to the oscillating tunnel experiment reported by van der Werf et al. (2007). In this case, the sediment bed consists of sand of mean diameter d_{50}=0.44 mm. The flow is driven by onshore-skewed velocity time series (Stokes 2nd order wave shape) of root-mean-square velocity amplitude 0.39 m/s and wave period of 5 sec. The simulation is initialized with a large ripple height of 0.11 m. After the simulation continues for about 8 wave periods, the model predicts a ripple geometry similar to the measured data with ripple steepness of 0.18, which is very close to the measured value of 0.17. We also validated the model for its velocity profiles and sediment concentration profiles and obtained very good agreement with measured data (Salimi-Tarazouj et al. 2020a).

Vorticity and sediment horizontal flux color contours during onshore deceleration phase are shown in Figure 22(b),(c) to illustrate how the local flow and vortices generated over the ripples can lead to horizontal sediment flux during the more intense onshore (wave crest) interval. These results are contrasted with the instant shown in Figure 22(d),(e) at the moment of weaker offshore deceleration phase (wave trough) in order to understand key processes leading to a net onshore ripple migration. Regions I and II (see Figure 22(c)) denote a major onshore near-bed flux generated due to intense boundary layer flow over stoss (offshore side) flank of the ripple followed by an ejection of sediments into the primary vortex. Region III denotes offshore-directed near-bed sediment flux due to the return flow of the primary vortex. Region IV shows onshore flux at lee flank due to avalanching when the ripple slope is too steep. The combination of intense boundary layer flow over the ripple, ejection and avalanching (I, II, V) causes major onshore sediment flux. On the other hand, major offshore sediment flux occurs during offshore acceleration phase when the large primary vortex generated during wave crest interval (region V) is ejected offshore. For the remaining offshore phases, the offshore transport is less intense than that during onshore phases and hence a net onshore transport occurs mainly as the near-bed sediment flux. In summary, when driven by onshore velocity-skewed wave motion, the near-bed load via ripple migration (see migration rate discussion in Figure 24(c)) is onshore-directed. On the contrary, suspended load transport is offshore-directed due to more intensive primary vortex generated during wave crest intervals. The opposite transport direction associated with near-bed load and suspended load due

to complex vortices evolution over the ripple bed is consistent with the laboratory observation reported by van der Werf et al. (2007).

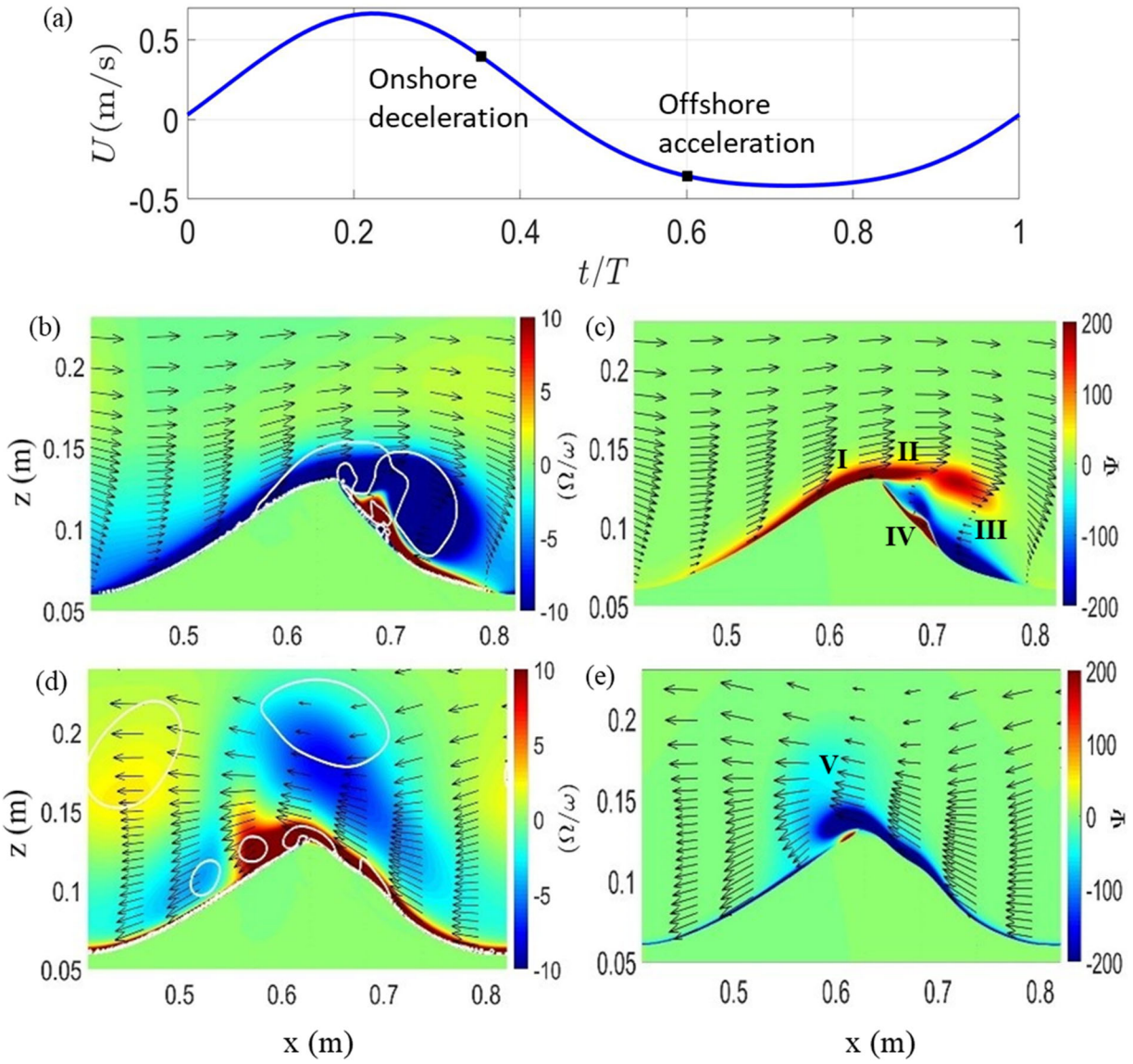

Figure 22: SedFoam simulation of sediment transport and migrating ripple driven by an onshore velocity skewed wave motion with its time series shown in panel (a). Panel (b), (c) show snapshots of vorticity and sediment horizontal flux color contour at the instant of onshore deceleration while panel (e), (f) show the corresponding color contour at the instant of offshore acceleration. I, II, III, IV and V in panel (c) and (e) indicated processes discussed in the text.

In the surf zone, breaking waves can cause a near bed velocity time series that is not only onshore velocity-skewed but also onshore acceleration-skewed. Therefore, it is also of interest to study how an onshore acceleration-skewed wave shape with zero velocity skewness (typically called a sawtooth wave shape, see Figure 23(a)) can drive ripple migration. Using the same grain size, wave period and root-mean-square velocity amplitude as the velocity-skewed case shown in Figure 22, we drive the model with an acceleration-skewed velocity time series (Figure 23(a)). Examining the contour plots of vorticity and sediment horizontal flux at an instant during onshore flow (crest) acceleration, it is clear that a large magnitude of onshore sediment flux is driven by strong accelerating bottom boundary layer flow over the ripple surface (negative vorticity in Figure 23(b)), which effectively carries sediment from the stoss (offshore) side of the ripple to the lee (onshore) side of the ripple (see Figure 23(c)). Interestingly, during the offshore acceleration instant, a similar offshore-directed flow and sediment flux are observed but with much weaker magnitude (see Figure 23(d),(e)). Due to this asymmetry in onshore/offshore sediment fluxes, which is clearly proportional to the intensity of acceleration, a net onshore transport and onshore migration is obtained. It is interesting to also point out that unlike the onshore velocity-skewed case shown in Figure 22, both near-bed load and suspended load are onshore-directed when driven by onshore acceleration-skewed waves.

By tracking the crest of the ripple profiles obtained at different wave cycle during the simulation for both velocity-skewed wave case (Figure 24(a)) and acceleration-skewed wave case (Figure 24(b)), we can calculate the ripple migration speed of these two cases (see Figure 24(c)). The migration speed for the onshore velocity-skewed case is about 16 mm/ min, which is very close to the measured data of 18 mm/min reported by van der Werf et al. (2007). For the acceleration-skewed wave case, onshore migration with a migration speed of 10 mm/min is obtained in the numerical simulation. In summary, SedFoam is capable of predicting ripple migration driven by nonlinear waves in the nearshore. Future work should focus on simulating how bedform migrations cause burial and reemergence of UXO along with other scour burial mechanisms.

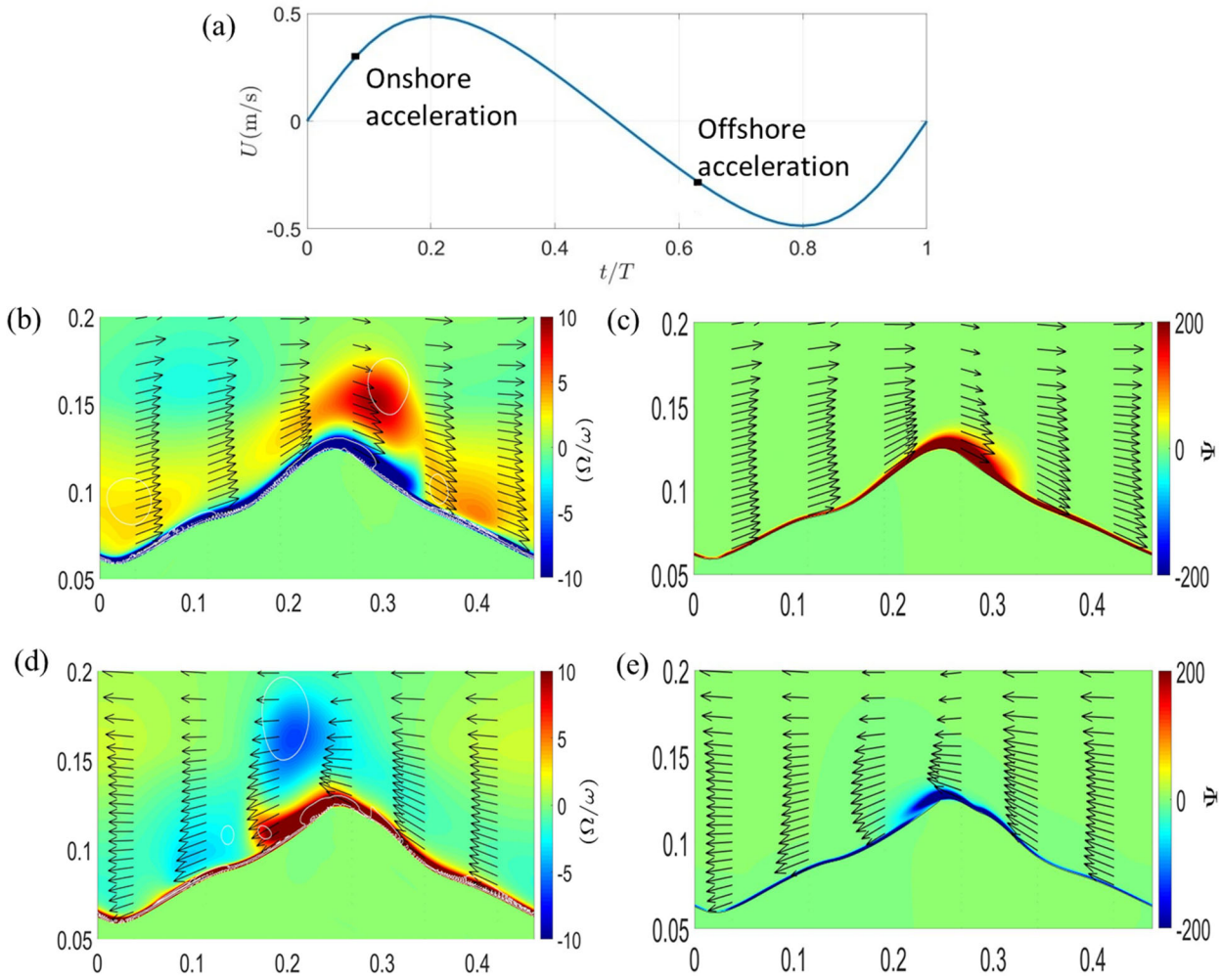

Figure 23: SedFoam simulation of sediment transport and migrating ripple driven by an onshore acceleration skewed wave motion with its time series shown in panel (a). Panel (b), (c) show snapshots of vorticity color contour and sediment horizontal flux at the instant of onshore deceleration while panel (e), (f) show the corresponding color contour at the instant of offshore acceleration. I, II, III, IV and V in panel (c) and (d) indicated processes discussed in the text.

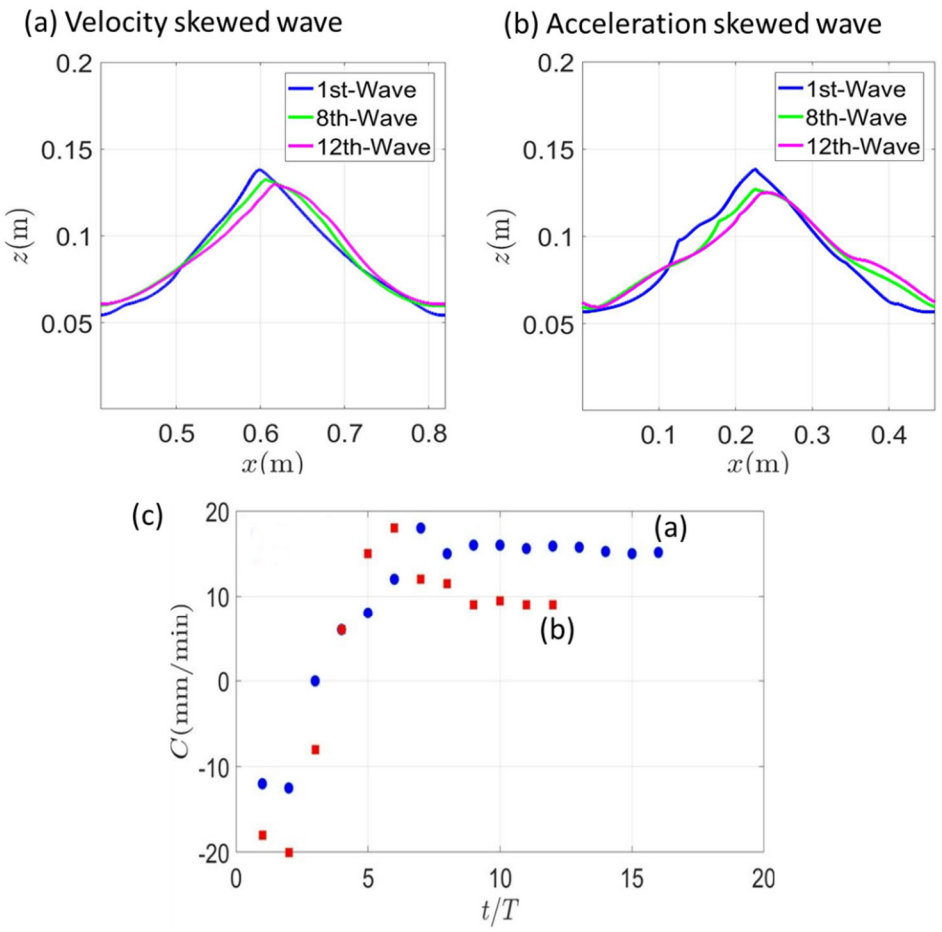

Figure 24: (a) Ripple profiles driven by onshore velocity-skewed waves at different wave cycle visualized using contour of volumetric concentration ϕ=0.57. (b) Ripple profiles driven by onshore acceleration-skewed waves at different wave cycle (c) Ripple (onshore) migration rate as a function of number of wave cycle for onshore velocity-skewed wave case (blue dots) and onshore acceleration-skewed wave case (red dots).

5. Conclusion and Implication for Future Research

Through the support of the 1-year SEED project, we delivered a validated SedFoam model capable of accurately and efficiently simulating several inter-connected vital processes between hydrodynamics, sediment transport, underwater objects and seabed response. A summary of major finding and research outcomes is given in Section 5.1. It is in our opinion that a more extensive effort is needed to integrate consistently these aforementioned key elements, along with a few other technical advancements, in the SedFoam modeling framework to create a new numerical modeling tool for scour burial of UXO. The new model can be used as a reliable analytical tool to study the mechanisms and thresholds for deep burial and the effect of munition density. Moreover, extensive and well-designed numerical simulations can be carried out to expand and to fill the gaps of scour burial data currently used in the UnMES. A brief discussion on future research is provided in Section 5.2.

5.1 Summary of Findings

A novel Eulerian two-phase numerical modeling framework for sediment transport applications, SedFoam, has been enhanced in this SEED project toward modeling deep scour burial of UXO. As a first step, the model has been successfully extended to capture dilatancy effects on sediment transport. The new sub-model has been validated for underwater avalanche and the model is able to reproduce the very slow increase of avalanche velocity in dense sediment concentration condition and much rapid increase of avalanche velocity in loose packing condition similar to the laboratory experiment measured by Pailha et al. (2008). Moreover, SedFoam is shown to be able to simulate the piping process by comparing with laboratory measured data reported in Sumer et al. (2001). Piping is the more realistic scour onset where the object is partially buried in the sediment bed initially. Direct simulation of piping is difficult to be achieved by conventional single-phase CFD models but it is demonstrated here as the strength of the present two-phase modeling approach.

Several proof-of-concept simulations show that SedFoam is capable of simulating scour driven by waves with realistic onset through piping and backfilling, scour of a 3D short cylinder at low to high KC number with similar scour pattern observed in the laboratory experiment of Dimer and Garcia (2007). The highest KC number run reaches the wave condition similar to the field observation reported at Duck, NC (Klammler et al. 2019) in sheet flow condition. The model is also capable of simulating migration and evolution of bedforms with migration speed similar to laboratory experiment and ripple geometry evolutions agree with empirical formulae.

We have fulfilled the project objectives to show that the Eulerian two-phase model SedFoam provides an effective modeling framework to directly resolve critical processes in scour, which cannot be achieved by conventional single-phase modeling approach. Moreover, several model enhancements and proof-of-concept simulations provide promising advancement for SedFoam and the model is now ready for a full implementation toward a new research tool for scour burial of UXO.

5.2 Opportunities for Future Research

The full implementation in SedFoam to solve deep burial problems allow the investigation of two critical physical mechanisms responsible for scour burial: 1) Mechanisms triggering deep scour burial (~1 meter), and 2) Effect of UXO density. Through extensive discussion with several

SERDP investigators, a consensus has emerged and it can be phrased into a *hypothesis* that deeper burial is related to UXO density, however, a mechanism (or mechanisms) must first exist to fluidize or liquefy the sediment bed. We would like to use the fully equipped SedFoam numerical modeling framework to investigate this critical problem. Essentially, we propose to use SedFoam as a research tool to create parameterizations for liquefaction potential, burial depth as a function of UXO density, and other nondimensional flow parameters (e.g., Shields parameter and KC number). We must point out that the full understanding of deep burial requires extensive field observation and they will be used to validate our numerical model. However, due to the high cost of field observation, it is very difficult to obtain sufficient amounts of data to complete the parametric space in order to train the probabilistic model UnMES (Rennie 2017). Well-designed numerical experiments can be carried out to fill the parameter space, either for higher quality interpolation within the range of the field observation, or for extrapolation to extreme events that are outside the range of field data. Simulation data will be made available to train the existing expert system UnMES for scour burial prediction. A flow chart for the proposed three-year project covering full modeling implementation, science goal and applications is presented in Figure 25.

To provide more details, a full implementation of SedFoam to solve scour burial problem with emphasis on deep burial require several technical tasks to be carried out in the near future:

1) From dilatancy/pore-pressure feedback to partially undrained soil response for high overburden

As mentioned before, to enhance a sediment transport model from surface transport (upper 10 cm of the seabed) to seabed stability and deep burial (~1 m in to the seabed) requires a rigorous and innovative merge between fluid mechanics and soil mechanics due to much higher overburden in deeper part of the sediment bed. We have carried out an inter-comparison between the present Eulerian two-phase mass and momentum equations with the well-known Biot's equations in soil mechanics. It is clear that by neglecting the nonlinear convection terms in the two-phase flow equations, which is appropriate for creeping motion in the transition from fluid-like to solid-like motion in high sediment concentration, the two-phase equations can be reduced to the Biot's equation except for a term associated with modeling a slight compressibility of the pore fluid due to a small air content.

According to our ongoing investigation on including the dilatancy effect discussed in Section 4.3, we have established that dilatancy is the volume change of granular materials due to micro-structure rearrangement. In other words, dilatancy and its effect occurs at sub-grid scale that cannot be directly resolved by the present two-phase equations derived by averaging over individual grain and pore. Hence, we adopt an empirical approach to model the effect of dilatancy and pore-pressure feedback. After including the slight compressibility (or called artificial compressibility) in the two-phase equation to deal with small air content in the soil, we may need to revise the sub-grid model for dilatancy and pore-pressure response. This integrated model improvement is essential to model partially-drained soil and liquefaction. We will expand the existing two-phase solver for hybrid incompressible and compressible flow. Within the OpenFoam framework, such a solver has been developed for fluidized bed (e.g., Ghione 2012; Manni 2014), and it can be extended for the present sediment transport/soil response application. After this important implementation is completed, we will further explore the model extension to unsaturated soil and soil with different amounts of fines (silt/clay) content within this modeling framework. Sand beds with different amounts of fines can cause very different water retention rates and hence these

different complexities are all inter-connected but the fundamental step is to first include solving water compressibility in the SedFoam modeling framework.

2) A complete and consistent description of sediment stresses for high overburden

As mentioned before, the advantage of the two-phase modeling framework is to be able to include various sediment phase stresses, which allows a full description of sediment transport without the conventional bedload and suspended load assumptions. However, the existing sediment stress closures in SedFoam are appropriate for transport near the surface layer of the sediment bed with very low overburden. For larger overburden, a more complete sediment stress description is needed. In the dilute to moderate sediment concentration, sediment stress is mainly caused by short-lived collision and turbulence. The kinetic/collisional component of sediment stress, either through kinetic theory or mu(I) rheology, are well-established in SedFoam and they generally show a shear thickening feature (effective viscosity becomes larger when driven by higher flow shear rate) in low to moderate concentration range. When sediment concentration is high, sediment stress is expected to show shear thinning behavior and eventually, sediment particles collectively show almost solid-like, elastic behavior in very high concentration with very low mobility and the granular skeleton supports nearly all the overburden. The particle pressure in the last stage of very high concentration is currently modeled by an empirical formulation of Johnson and Jackson (1987) which demonstrates the expected elastic behavior at low overburden. In the particle shear stress counterpart, the transition from plastic to elastic behavior of sediment grains are modeled empirically to match a qualitative shear-thinning features and eventually leading to an immobile bed (Srivastava and Sundaresan 2003). For larger overburden, a more rigorous elastic stress model based on Hooke's law needs to be incorporated. It may be also useful to explicitly include a shear thinning formulation in moderate to high sediment concentration based on Herschel-Bulkley model.

3) Numerical implementation of moving objects.

A realistic scour burial simulation of UXO requires direct modeling of the movement of UXO as the sediment bed is eroded, or more generally as the sediment bed is fluidized or liquefied, the relatively densities between UXO and soil can lead to the sinking or floating of UXO. While all the essential physics on sediment transport and soil stabilities have been and will be incorporated in this project, it is also essential to include the model's capability for object movement subject to the law of momentum balance. Since SedFoam is created in the OpenFOAM framework, implementing moving objects is feasible as there are several options currently available in the OpenFOAM toolbox (e.g., Paci 2018). We are currently evaluating the most viable method for the present two-phase flow formulation.

4) Model validation with laboratory experiments and SERDP-supported field observation.

Once the model enhancement is completed, the most important next step is to validate the model for scour burial. Established upon our existing experience on simulating the scour of 3D short cylinders (see Section 4.5) for a range of KC numbers, we will validate the model with several scour burial laboratory and field datasets. For low to intermediate KC numbers, we will validate the model with scour burial data reported by Demir and Garcia (2007). For high KC numbers, especially related to deep burial and the possibility of liquefaction, we will validate the model with field observation reported by Klammler et al. (2019) and ongoing field observation to be carried out by Dr. Calantoni's group (Naval Research Laboratory).

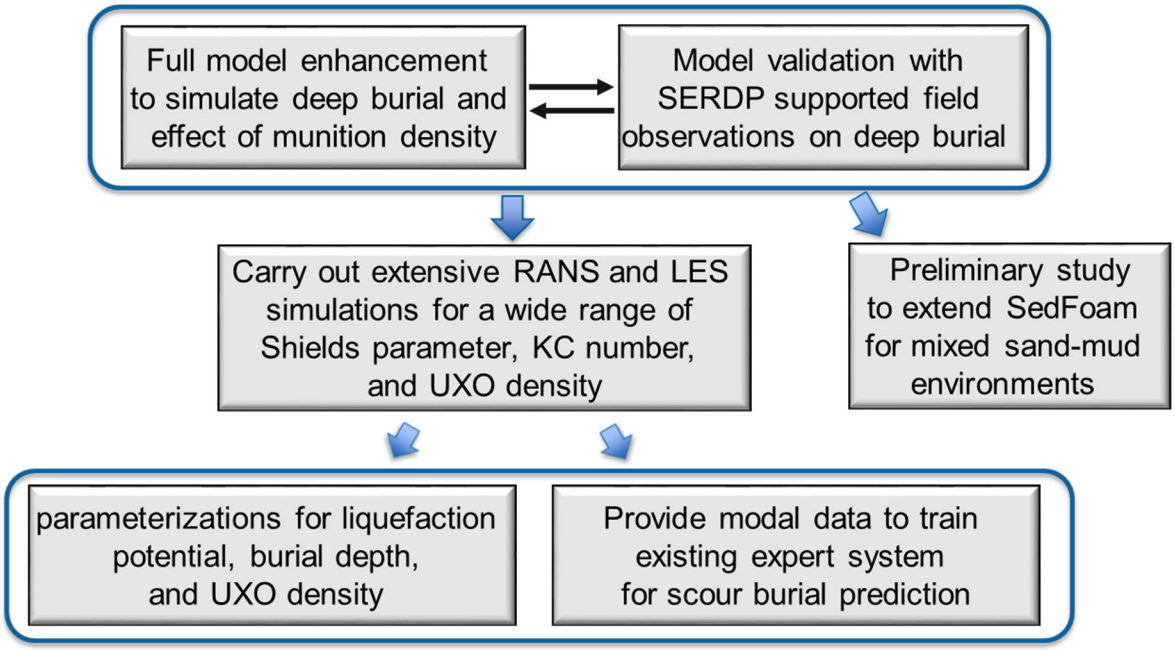

Figure 25: Flow chart of planned future investigation on scour burial process using SedFoam

6. Literature Cited

Baykal, C., Sumer, B. M., Fuhrman, D. R., Jacobsen, N. G., Fredsøe, J., (2015) Numerical investigation of flow and scour around a vertical circular cylinder. Philosophical Transactions of the Royal Society of London A: Mathematical, Physical and Engineering Sciences 373 (2033), 20140104.

Boyer, F., Guazzelli, E., Pouliquen, O., (2011) Unifying suspension and granular rheology, Phys. Rev. Lett. 107, 188301.

Calantoni, J., (2016) Long Time Series Measurements of Munitions Mobility in the Wave Current Boundary Layer, SERDP Project MR-2320, In-Progress Review.

Cataño-Lopera, Y.A. & García, M.H. (2006) Burial of short cylinders induced by scour under combined waves and currents. ASCE Journal of Waterway Port Coastal and Ocean Engineering 132(6): 439-449.

Cataño-Lopera, Y.A., Demir, S.T. & García, M.H. (2007) Self burial of short cylinders under oscillatory flows and combined waves plus currents. IEEE Journal of Oceanic Engineering, 32(1): 191-203.

Chauchat, J., Cheng, Z., Nagel, T., Bonamy, C., Hsu, T.-J. (2017) SedFoam-2.0: a 3-D two-phase flow numerical model for sediment transport, Geoscientific Model Development, 10, 4367-4392, doi:10.5194/gmd-10-4367-2017

Chauchat, J., (2018) A comprehensive two-phase flow model for unidirectional sheet-flows. J. Hydraul. Res. 1–14 .

Cheng, Z., Hsu, T.-J., Calantoni, J. C., (2017) SedFoam: A multi-dimensional Eulerian two-phase model for sediment transport and its application to momentary bed failure, Coastal Engineering, 119, 32-50, doi:10.1016/j.coastaleng.2016.08.007.

Cheng, Z., Chauchat, J., Hsu, T.-J., Calantoni, J. (2018) Eddy interaction model for turbulent suspension in Reynolds-averaged Euler–Lagrange simulations of steady sheet flow, Advances in Water Resources, 111, 435-451.

Chou, Y. J., & Fringer, O. B. (2010). A model for the simulation of coupled flow-bed form evolution in turbulent flows. Journal of Geophysical Research: Oceans, 115(10), 1–20.

Demir, S.T. & García, M.H. (2007) Experimental studies on burial of finite-length cylinders under oscillatory flow. ASCE Journal of Waterway Port Coastal and Ocean Engineering 133(2): 117-124.

Ding, J., & Gidaspow, D. (1990). A bubbling fluidization model using kinetic theory of granular flow. AIChE Journal, 36(4), 523–538. https://doi.org/10.1002/aic.690360404

Foster, D. L., A. J. Bowen, R. A. Holman, and P. Natoo (2006), Field evidence of pressure gradient induced incipient motion, J. Geophys. Res., 111, C05004, doi:10.1029/2004JC002863.

Friedrichs, C. T., Rennie, S. E., Brandt, A. (2016) Self-burial of objects on sandy beds by scour: A synthesis of observation. In (Harris, J., Whitehouse, R., Moxon, S., eds.) Scour and Erosion, CRC Press, p. 179-189.

Ghione, A. (2012) Development and validation of a two-phase CFD model using OpenFOAM. Master of Science Thesis, Division of Nuclear Reactor Technology, Royal Institute of Technology, Stockholm, Sweden.

Hsu, T.-J., Jenkins, J.T., Liu, P.L.-F., (2004) On two-phase sediment transport: sheet flow of massive particles. Proc. R. Soc. London Ser. A 460 (2048), 2223–2250.

Jenkins, J. T., Hanes, D. M., (1998) Collisional sheet flows of sediment driven by a turbulent fluid. J. Fluid Mech. 370, 29–52.

Johnson, P.C., Jackson, R., (1987) Frictional-collisional constitutive relations for gran- ular materials, with application to plane shearing. J. Fluid Mech. 176, 67–93.

Kim, Y., Cheng, Z., Hsu, T.-J., & Chauchat, J. (2018). A numerical study of sheet flow under monochromatic nonbreaking waves using a free surface resolving Eulerian two-phase flow model. Journal of Geophysical Research: Oceans, 123, 4693–4719

Kim, Y., Mieras, R. S., Cheng, Z., Anderson, D., Hsu, T.-J., Puleo, J. A., Cox, D. (2019) A numerical study of sheet flow driven by velocity and acceleration skewed near-breaking waves on a sandbar using SedWaveFoam, Coastal Engineering, 152, 103526.

Klammler, H, Sheremet, A., Calantoni, J. (2018) Seafloor burial of surrogate UXO by wave-induced sediment instability, IEEE J. Oceanic Eng., 45(3), 927-936.

Lun, C. K. K., Savage, S. B., Je_rey, D. J. & Chepurniy, N. (1984), Kinetic theories for granular flow: inelastic particles in Couette ow and slightly inelastic particles in a general flow field, Journal of Fluid Mechanics 140, 223-256.

Manni A. (2014) An introduction to twoPhaseEulerFoam with addition of a heat exchange model, Chalmers University of Technology, Gothenburg, Sweden.

Marieu, V., Bonneton, P., Foster, D. L., & Ardhuin, F. (2008). Modeling of vortex ripple morphodynamics. Journal of Geophysical Research: Oceans, 113(9), 1–15.

Marzougui, Donia, Chareyre, Bruno & Chauchat, Julien (2015) Microscopic origins of shear stress in dense fluid–grain mixtures. Granular Matter 17 (3), 297–309.

Mogridge, G. R., M. Davies, and D. Willis (1994), Geometry prediction for wave-generated bedforms, Coastal Eng., 22(3–4), 255– 286.

Nagel, T., Chauchat, J., Bonamy, C., Liu, X., Cheng Z., Hsu T.-J. (2020) Three-dimensional scour simulations with a two-phase flow model, Advances in Water Resources, 138, 103544.

Pailha, M., Nicolas, M. & Pouliquen, O. (2008) Initiation of underwater granular avalanches: influence of the initial volume fraction. Phys. Fluids 20, 111701.

Paci, A. (2018) Numerical analysis of floating structures for off-shore and harbor Engineering, Master Thesis, Universitá di Bologna, Bologna, Italy.

Pailha, M., Pouliquen, O., (2009) A two-phase flow description of the initiation of underwater granular avalanches, J. Fluid Mech., 633, 115-135.

Rennie, S. E., (2017) Underwater munitions expert system to predict mobility and burial, SERDP Project Report MR-2227.

Rennie, S.E., A. Brandt, C.T. Friedrichs, (2017). Initiation of motion and scour burial of objects underwater, Ocean Engineering, Vol 131, 282-294.

Rognon, Pierre, Einav, Itai & Gay, Cyprien (2011) Flowing resistance and dilatancy of dense suspensions: lubrication and repulsion, J. Fluid Mech., 689, 75-96.

Roulund, A. , Sumer, B. , Fredsøe, J. , Michelsen, J. , (2005) Numerical and experimental investigation of flow and scour around a circular pile. J. Fluid Mech. 534, 351–401.

Salimi-Tarazouj, A., Hsu, T.-J., Traykovski, P., Cheng, Z., Chauchat, J. (2020a) A numerical study of wave orbital ripples using a Eulerian two-phase model – Analyses on intra-wave sediment transport, submitted to J. Geophys. Res.

Salimi Tarazouj, A., Hsu, T.-J., Traykovski, P., Cheng, Z., Chauchat, J. (2020b) A numerical study of wave orbital ripples using a Eulerian two-phase model – ripple evolution, in preparation.

Srivastava, A. and Sundaresan, S. (2003) Analysis of a frictional-kinetic model for gas-particle flow, Powder Technol., 129, 72–85.

Sumer, B. M., Truelsen, C., Sichmann, T., Fredsoe, J., (2001) Onset of scour below pipelines and self-burial, Coastal Eng., 42, 313-335.

Traykovski, P. 2007. Observation of wave orbital scale ripples and a nonequilibrium time-dependent model, J. Geophys. Res., 112, C06026, doi:10.1029/2006JC003811.

Traykovski, P., Hay, A. E., Irish, J. D., & Lynch, J. F. (1999). Geometry, migration, and evolution of wave orbital ripples at LEO-15. Journal of Geophysical Research: Oceans, 104(C1), 1505–1524.

Traykovski, P., T. Austin, (2017) Continuous Monitoring of Mobility, Burial, and Re-Exposure of Underwater Munitions in Energetic Near-Shore Environments, SERDP Project MR-2319, Final Report, 44pp.

van der Werf, J. J., J. S. Doucette, T. O'Donoghue, and J. S. Ribberink (2007) Detailed measurements of velocities and suspended sand concentrations over full-scale ripples in regular oscillatory flow, J. Geophys. Res., 112, F02012, doi:10.1029/2006JF000614.

Wiberg, P. L., Harris, C. K., (1994) Ripple geometry in wave-dominated environemtns, J. Geophys., Res., 99(C1), 775-789.

Wilkens R. H. and M. D. Richardson, Guest Editorial Special Issue on Mine Burial Processes, in IEEE Journal of Oceanic Engineering, vol. 32, no. 1, pp. 1-2, Jan. 2007, doi: 10.1109/JOE.2007.890937.